A general framework for the simulation of geochemical compaction

Bianca Giovanardi[1] · Anna Scotti[1] · Luca Formaggia[1] · Paolo Ruffo[2]

Received: 26 November 2014 / Accepted: 24 July 2015 / Published online: 22 August 2015

1 Introduction

The study of compaction processes occurring in rock lay-ers during sedimentation is relevant to study, for instance, the distribution of possible over-pressures and of the induced variation of porosity and permeability. Together with the mechanical processes, compaction and overpres-sure are affected by fluid $\leftrightarrow$ solid conversion through two basic mechanisms. Firstly, fluid production/consumption by chemical reactions acts as a source/sink term and may cause changes in the fluid pressure and thus in the effective stress. Secondly, dissolution/precipitation mechanisms alter the solid matrix porosity, and consequently permeability, in the areas where the reactions occur.

It is well known that porosity is influenced by the local stess field. In particular, the Terzaghi assumption postulates the existence of a relation of the type $\phi = \phi(\sigma)$, where ϕ is the porosity and σ the effective stress, which in the simpler cases is taken to be $\sigma = s - \alpha p_f$, s being the overburden, or more precisely the vertical stress, and p_f the pore fluid pressure. Here, the Biot-Willis coefficient [2] α is a parameter that accounts for grain-to-grain interfa-cial area. Its expression is $\alpha = 1 - K_d/K_s$, where K_d and K_s are the bulk modulus of the drained rock and of the

MOX Politecnico di Milano - Dipartimento di Matematica,
Web-site: http://mox.polimi.it; E-mail: lab-mox@polimi.it

✉ Bianca Giovanardi
bianca.giovanardi@polimi.it

Anna Scotti
anna.scotti@polimi.it

Luca Formaggia
luca.formaggia@polimi.it

Paolo Ruffo
paolo.ruffo@eni.com

[1] Department of Mathematics, Politecnico di Milano, Via Edoardo Bonardi 9, Milano,
Mi 20133, Italy

[2] Exploration, RIGE Department, Eni S.p.A.,
5° Palazzo Uffici – Room 4046 E, Via Emilia 1,
20097 San Donato Milanese MI, Italy

solid grains, respectively. In our numerical experiments, for the sake of simplicity, we have taken $\alpha = 1$, which corresponds to incompressible solid grains, yet the proposed model accounts for any value of α.

Different relations and rheological laws have been proposed for this type of problem, as in [13, 14, 25, 29]; however, algebraic laws that relate porosity to effective stress directly are still the most used in practice, since they are easy to calibrate. In particular, to describe mechanical compaction, we make use of Athy's law $\phi = \phi_0 e^{-\beta\sigma}$, even if the proposed scheme may be readily adapted to other algebraic relations $\phi = \phi(\sigma\ )$. Extensions to viscous or viscoelastic relations are still possible but they require more extensive changes in the scheme. We also point out that the use of a simple compaction law that only depends on the vertical effective stress is a reasonable approximation for basins that do not exhibit inherently three-dimensional features such as faults, salt-diapirism, extensional behavior. In the aforementioned cases, the formation and dynamics of basins have been successfully modeled with a stratified fluid model, see [17, 19].

We then account for chemical reactions using simpli-fied chemical kinetics describing the conversion of either a solid matrix into a fluid, like in kerogen-oil conversion (see [22, 24]), or the precipitation of a mineral solute, such as quartz (see [15, 18]). We follow the model proposed in [27] assuming vertical compaction and recasting the gov-erning equations in a Lagrangian frame. The effect of the fluid-solid conversion on porosity is accounted for by a suitable modification of the constitutive law for ϕ. We simu-late the sedimentation process by providing a sedimentation rate, yet we assume that the rock layer under considera-tion has already been buried at the start of the simulation. Therefore sedimentation effectively acts as a variation of the overburden.

In this work, we present in detail a numerical scheme for the solution of the set of differential equations governing the problem, which comprises chemical reaction, rock displacement, and flow in the porous matrix, with permeability depending on the porosity. For the sake of simplicity, we have assumed a given temperature field, which may, however, vary in space and time, yet the addition of the energy equation would not cause major difficulties. We have also adopted a rather simple model for the chemical reactions. Again, it is possible to use more complex models within the same methodological framework. The aim of this work, however, is to investigate the coupling effects among flow, deformation and reaction, at the expense of some simplifications in the model and in the geometry of the test cases. Commercial software (such as VISAGE) are indeed available to simulate sediments dynamics, including compaction, on complex geometries. However, they are designed to model dynamics at a much shorter time scale, i.e., that of reservoir exploitation, and do not account for porosity changing reactions. Conversely, software for reactive transport such as TOUGHREACT can account for multiphase-multicomponent problems and simulate mineral dissolution/precipitation on fixed domains.

We propose a splitting strategy, as it has been done in [9], that allows to treat each differential problem with an appropriate numerical scheme. In particular, we have used mixed finite elements for the Darcy equations and a mass preserving monotone scheme for the saturation equation. The reason for choosing a splitting strategy is that for more realistic computations, one may want to use already available code with minimal modifications. We have cast the procedure in rather general frame so to be able to treat the different situations of mineral precipitation and kerogen conversion. Stability has been gained by choosing a suitable time discretization of the continuity equation. Care has been taken to control mass imbalance linked to the splitting. We show with numerical experiments that the splitting is stable and able to describe the phenomena correctly.

The paper is organized as follows. In Section 2, we present the mathematical model and the derivation of the various equations. Section 3 describes the proposed numerical discretization in details for the case of mineral precipitation, while Section 4 deals with the specialization to kerogen conversion. Section 5 illustrates three different strategies for the discretization of the continuity equation in both the two cases. Some numerical results are shown in Sections 6 and 7, while conclusions are drawn in Section 8.

2 A basic model

The objective of this section is to outline a mathematical model for compaction in sedimentary rocks that accounts for porosity changes due to chemical effects, such as solid-fluid conversion process. The model that we are going to describe is rather general and can be representative of all processes that involve conversion to liquid of part of the solid matrix (e.g., in case of kerogen degradation in source rock) and precipitation of part of the fluid in pores on the solid matrix of the rock (e.g., in case of mineral precipitation in sandstone rocks).

We consider an open-bounded domain $\Omega \subset \mathrm{IR}^2$ with coordinate system $(x,\ z)$, yet the derivation can be read-ily extended to the $3D$ case. In particular, we consider a two-dimensional cross section of a layer within a sedimentary basin. The rock is assumed to consist of three basic parts: inert part of rock that does not undergo any solid-fluid conversion, rock subject to dissolution and precipitation, and a void part initially filled with water. The inert mineral part and the reactive part of the rock together form the

solid sediment matrix. We point out that, due to dissolution/precipitation events and to mechanical compaction, the solid matrix evolves in time.

The flow is assumed to obey Darcy's law. To derive the model, we introduce some additional hypotheses. The first is that the compaction process is governed by the same basic mechanisms that give rise, when only mechanical compaction is present, to Athy's law of mechanical compaction (see [27] and [28]).

The second hypothesis is that the dissolvable part of the rock can be considered distributed in the solid matrix. Indeed, following [27] and [28], we assume that at any point $\mathbf{x}$ inside the domain and at any time t, we can define a field $C = C(\mathbf{x}, t)$ that represents the volume fraction of reactive rock with respect to the initial state.

We also make the usual assumption that compaction only acts vertically. The extension to more general situations is possible but, because of its complexity, is beyond the scope of this paper.

In the following sections, we will sometimes make use of some standard notations of functional spaces. We recall here the basic definitions, the interested reader may find more precise and complete details in, for instance, [4] or [23]. Given a domain $\Omega \subset \mathbb{R}^d$, with d either 1 or 2, we indicate with $C^k(\Omega)$ the space of functions in Ω continuous up to the kth derivative. While, $L^2(\Omega)$ is the space of square-integrable functions, i.e., functions v for which $\int_\Omega v^2 \, d\Omega$ exists and is finite and $L^\infty(\Omega)$ is the space of bounded functions in Ω. With $H^1(\Omega)$, we indicate the space of function in $L^2(\Omega)$ with all first derivatives in $L^2(\Omega)$ and with $W^{1,\infty}(\Omega)$ the space of function in $L^\infty(\Omega)$ with first derivatives in $L^\infty(\Omega)$ (i.e., bounded functions with bounded first derivatives). In the case of vector functions, like displacements or velocities, the above definitions are applied to each component. The space $H(div, \Omega)$ is the space of vector functions in $L^2(\Omega)$ with divergence in $L^2(\Omega)$, it is the natural functional space for the Darcy's velocity field.

2.1 Rock description and coordinates

Because of the solid-fluid conversions and of the compaction of the rock due to the vertical stress, the solid matrix is not fixed and the domain Ω is time dependent. To avoid this complication and write the equations on a fixed domain, we follow [27] and introduce the auxiliary domains $\Omega^*(t)$ and $\hat{\Omega}$, whose coordinates will be indicated in the following with (x, η) and (x, ξ), respectively. Notice that, since we assume that compaction leads only to a vertical movement of the solid matrix, all the domains share the same coordinate x. Fixed the time instant t, $\Omega^*(t)$ is obtained from the actual domain $\Omega(t)$ as its completely compacted configuration, while $\hat{\Omega}$ is obtained from $\Omega^*(t)$ by removing the reactive part of the rock. Thus, $\hat{\Omega}$ represents the volume occupied by inert material and is fixed with time. Indeed, the ξ coordinate is neither influenced by compaction of the sediment column due to the overburden nor by the fact that a part of the solid sediment skeleton can dissolve into the fluid. For these reasons, we choose it as the Lagrangian coordinate of our model.

We recall that we are studying the evolution of a single sedimentary layer, which moreover has already been buried at the initial time. Thus, the sedimentation of the overlying layers is only taken into account by a suitable modification of the boundary conditions and of the overburden, without the addition of material to the domain of interest.

Let z be the vertical coordinate which has the bottom layer as the origin and ξ be the coordinate that measures the height of the non-dissolvable part of the completely compacted rock and has the bottom layer as the origin (see Fig. 1). Both axes are oriented upwards.

As explained in [27], the map $\boldsymbol{\varphi}_t : \hat{\Omega} \to \Omega(t)$, $\boldsymbol{\varphi}_t(x, \xi) = (x, z(\xi, t))$ is given by

$$\boldsymbol{\varphi}_t(x, \xi) = \left(x, \; z_{top}(x, t) - \int_\xi^{\xi^*(x)} \frac{1 - C_0(x, \xi') + C(x, \xi', t)}{(1 - C_0(x, \xi'))(1 - \phi(x, \xi', t))} \mathrm{d}\xi' \right), \tag{1}$$

where $\xi^*(x)$ is the height of the layer along the ξ-axis and is computed knowing the porosity and the concentration field at the initial configuration. z_{top} is the height of the domain along the z-axis and may depend on time. Finally, $C_0(x, z) = C(x, z, 0)$, and ϕ is the porosity.

In fact, fixed the x-coordinate and the time instant t, in a small sediment section of thickness $\mathrm{d}z$ the thickness of the fully compacted solid is given by

$$\mathrm{d}\eta = (1 - \phi) \, \mathrm{d}z. \tag{2}$$

The thickness of the section measured as compacted rock without any degradable material is

$$\mathrm{d}\xi = (1 - C_0) \, \mathrm{d}\eta_0, \tag{3}$$

where C_0 is the initial volume fraction of the reactive material and $\mathrm{d}\eta_0$ is the initial amount of solid sediment.

Since

$\mathrm{d}\eta = (1 - C_0 + C) \, \mathrm{d}\eta_0$, (4) by inserting Eq. 4 in Eq. 3 and considering Eq. 2, we obtain

$$\mathrm{d}\xi = \frac{1 - C_0}{1 - C_0 + C} \mathrm{d}\eta = \frac{(1 - C_0)(1 - \phi)}{1 - C_0 + C} \mathrm{d}z. \tag{5}$$

Thus, it follows that

$$\frac{\partial z}{\partial \xi} = \frac{1 - C_0 + C}{(1 - C_0)(1 - \phi)}. \tag{6}$$

Integrating between ξ and ξ^*, we obtain the relationship between z and ξ, that is

$$z = z_{top} - \int_\xi^{\xi^*} \frac{1 - C_0 + C}{(1 - C_0)(1 - \phi)} \mathrm{d}\xi'. \tag{7}$$

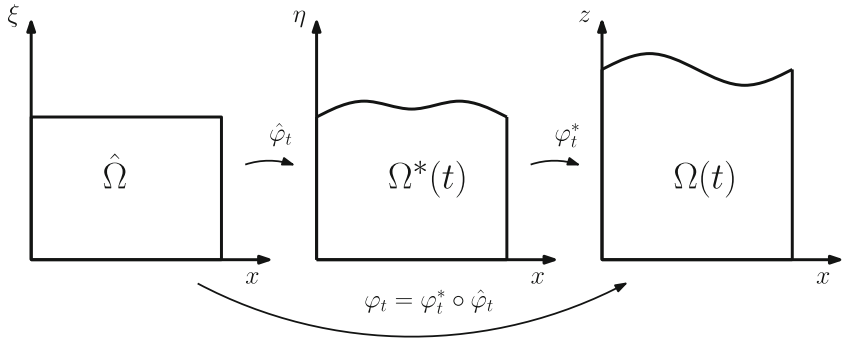

Fig. 1 The three coordinates systems. On the right, the physical domain $\Omega(t)$. The domain $\Omega^*(t)$ is obtained from $\Omega(t)$ as its completely compacted configuration, and $\hat{\Omega}$ is obtained from $\Omega^*(t)$ by removing all the reactive part of the rock

Remark 1 Notice that, under some restrictive hypotheses, $\boldsymbol{\varphi}_t$ is actually a change of coordinates. In fact, since both $\frac{1-C_0+C}{(1-C_0)(1-\phi)}$ and $\frac{(1-C_0)(1-\phi)}{1-C_0+C}$ are positive, $\boldsymbol{\varphi}_t$ is bijective. Moreover, if $C_0 \in C^0(\Omega)$ and $\phi \in C^0(\Omega)$ then $\boldsymbol{\varphi}_t \in C^1(\Omega)$. Finally, the deformation gradient F of the map $\boldsymbol{\varphi}_t$ is

$$\mathsf{F} := \nabla \boldsymbol{\varphi}_t = \begin{bmatrix} 1, & 0 \\ \partial z/\partial x, & \partial z/\partial \xi \end{bmatrix}. \tag{8}$$

and

$$J := \det(\mathsf{F}) = \frac{\partial z}{\partial \xi} = \frac{1 - C_0 + C}{(1 - C_0)(1 - \phi)} > 0. \tag{9}$$

Let us observe that, due to the choice of the reference configuration $\hat{\Omega}$, the time derivative of the map from the reference to the actual configuration coincides with the velocity of the solid matrix, i.e., $\frac{\partial \boldsymbol{\varphi}_t}{\partial t} = \mathbf{u}_s$. We point out that, due to the hypothesis of vertical compaction, one has $\mathbf{u}_s = u_{sz}\, \mathbf{e}_z$, where $\mathbf{e}_z$ is the unit vector of the z-axis.

Finally, $\frac{\partial z}{\partial x}$ is given by

$$\frac{\partial z}{\partial x} = \frac{\partial z_{top}}{\partial x} - \frac{1 - C_0(\xi^*) + C(\xi^*)}{(1 - C_0(\xi^*))(1 - \phi(\xi^*))} \frac{\partial \xi^*}{\partial x} - \int_{\xi}^{\xi^*(x)} \frac{\partial}{\partial x} \left(\frac{1 - C_0 + C}{(1 - C_0)(1 - \phi)} \right) \mathrm{d}\xi'. \tag{10}$$

Remark 2 If C_0 is in $L^\infty(\hat{\Omega})$, C, ϕ are in $L^\infty(\hat{\Omega})$ for each t, and

$$\frac{\partial z}{\partial x} \in L^\infty(\hat{\Omega}), \quad \frac{\partial \xi^*}{\partial x} \in L^\infty(\hat{\Omega}),$$

$$\frac{\partial}{\partial x} \left(\frac{1 - C_0 + C}{(1 - C_0)(1 - \phi)} \right) \in L^\infty(0, \xi^*(x)),$$

$$\frac{\partial}{\partial x} \left(\frac{(1 - C_0)(1 - \phi)}{1 - C_0 + C} \right) \in L^\infty(0, z_{top}(x, t)),$$

then $\boldsymbol{\varphi}_t \in W^{1,\infty}(\hat{\Omega})$ and $\boldsymbol{\varphi}_t^{-1} \in W^{1,\infty}(\Omega(t))$ for all $t \in (0, T)$. In this case, it can be shown (see [12] for the proof) that $\hat{v} = v \circ \boldsymbol{\varphi}_t \in H^1(\hat{\Omega})$ if and only if $v \in H^1(\Omega(t))$. Moreover, $||v||_{H^1(\Omega(t))}$ is equivalent to $||\hat{v}||_{H^1(\hat{\Omega})}$.

We conclude this section by observing that a generic partial differential equation in conservation form

$$\frac{\partial g}{\partial t} + \nabla \cdot (g\mathbf{u}) = Q \qquad \text{in } \Omega(t) \times (0, T), \tag{11}$$

with $g = g(x, z, t)$, can be formulated in the fixed reference system as

$$\frac{\partial (\hat{g}\hat{J})}{\partial t} + \hat{\nabla} \cdot (\hat{g}(\hat{\mathbf{u}} - \hat{\mathbf{u}}_s)) = \hat{Q}\, \hat{J} \qquad \text{in } \hat{\Omega} \times (0, T), \tag{12}$$

where here and in the following we set, for a generic function f, $\hat{f} = f \circ \boldsymbol{\varphi}_t$, for a generic velocity vector $\hat{\mathbf{v}} = \hat{J}\, \hat{\mathbf{F}}^{-1} \mathbf{v} \circ \boldsymbol{\varphi}_t$, and we have defined the operator

$$\hat{\nabla} = \begin{pmatrix} \partial/\partial x \\ \partial/\partial \xi \end{pmatrix} = \hat{\mathbf{F}} \nabla = \hat{\mathbf{F}} \begin{pmatrix} \partial/\partial x \\ \partial/\partial z \end{pmatrix}. \tag{13}$$

2.2 The governing equations

In the two-dimensional domain $\Omega(t)$ and in the assumption of vertical compaction, mass conservation for the solid implies

$$\frac{\partial}{\partial t} ((1 - \phi)\rho_s) + \frac{\partial}{\partial z} ((1 - \phi)\rho_s u_{sz}) = Q_s, \tag{14}$$

in $\Omega(t) \times (0, T)$, where Q_s is a source/sink term that models solid $\leftrightarrow$ fluid conversions.

The solid matrix density ρ_s in Eq. 14 is the mean over the densities of the two solid components, i.e., the inert one and the reactive one, weighted with their respective volume fractions, that is

$$\rho_s = \frac{(1 - C_0)\rho_r + C\rho_d}{1 - C_0 + C}. \tag{15}$$

From Section 2.1, it follows that Eq. 14 can be formulated in $\hat{\Omega} \times (0, T)$ as

$$\frac{\partial}{\partial t} \left((1 - \hat{\phi})\hat{\rho}_s \hat{J} \right) = \hat{Q}_s\, \hat{J}. \tag{16}$$

From Eq. 16, we can obtain an expression for $Q_s = Q_s(\phi, C)$. Indeed, since

$$\hat{J} = \frac{1 - \hat{C}_0 + \hat{C}}{(1 - \hat{C}_0)(1 - \hat{\phi})}, \tag{17}$$

Eq. 16 can be rewritten as

$$\frac{\partial}{\partial t}\left(\hat{\rho}_s \frac{1-\hat{C}_0(x,\xi)+\hat{C}(x,\xi,t)}{(1-\hat{C}_0(x,\xi))}\right) = \hat{Q}_s\ \hat{J}. \tag{18}$$

Using Eq. 15, we obtain

$$\frac{\partial}{\partial t}\left(\rho_r + \frac{\hat{C}(x,\xi,t)}{1-\hat{C}_0(x,\xi)}\rho_d\right) = \hat{Q}_s\ \hat{J}. \tag{19}$$

Thus, since both ρ_r and ρ_d are constant, rearranging the expression and substituting $\hat{J}$, we finally have

$$\hat{Q}_s = \rho_d \frac{(1-\hat{\phi})}{1-\hat{C}_0+\hat{C}}\frac{\partial \hat{C}}{\partial t}. \tag{20}$$

which, brought back to the current domain provides the following relation

$$Q_s = \rho_d \frac{1-\phi}{1-C_0+C}\frac{DC}{Dt}, \tag{21}$$

where $\frac{DC}{Dt} = \frac{\partial \hat{C}}{\partial t} \circ \boldsymbol{\varphi}_t^{-1}$. As expected, if $\frac{DC}{Dt} > 0$, then $Q_s > 0$ is a source term for Eq. 14, while, if $\frac{DC}{Dt} < 0$, then $Q_s < 0$ is a sink term. Here, $\frac{DC}{Dt}$ will be computed according to the geological processes of our interest.

We formulate the mass conservation of water in pores in a general way, to account for both the case where the dissolution of the rock induces a two-phase flow, as in the case of kerogen degradation into oil, and that where the dissolved material is transported by a single phase flow, as in the case of mineral dissolution/precipitation in flowing water. For this reason, we introduce the water saturation S_w, with the understanding that S_w is a variable only in the first case, while $S_w \equiv 1$ in the second one.

Mass conservation of water in $\Omega(t) \times (0,T)$ can be expressed as:

$$\frac{\partial}{\partial t}(\phi\rho_w S_w) + \nabla\cdot(\phi\rho_w S_w \mathbf{u}_w) = Q_w, \tag{22}$$

where $\rho_w = \rho_w(x,z,t)$ is the water density, which may depend on temperature and pressure, and $\mathbf{u}_w = \mathbf{u}_w(x,z,t)$ its velocity. In the following, we will assume that $Q_w = 0$, i.e., no water is released by reactions or injected.

The relative velocity $\mathbf{u}_w - \mathbf{u}_s$ of water with respect to the solid matrix is prescribed in $\Omega(t) \times (0,T)$ by Darcy law as

$$\phi S_w(\mathbf{u}_w - \mathbf{u}_s) = -\frac{k_{r,w}\mathsf{K}}{\mu_w}\left(\nabla p_w - \rho_w \mathbf{g}\right), \tag{23}$$

being $\mathbf{g} = -g\mathbf{e}_z$ the gravity acceleration. Here, $k_{r,w} = k_{r,w}(S_w) > 0$ is the relative permeability of water and is a given function of the saturation S_w with $k_{r,w}(1) = 1$, again to maintain a general framework. Finally, μ_w denotes the water viscosity, which may depend on temperature, and K is a symmetric positive definite permeability tensor, which depends on the porosity ϕ according to

$$\mathsf{K}(\phi) = \mathscr{K}(\phi)\begin{bmatrix} k_{xx}, & k_{xz} \\ k_{zx}, & k_{zz}\end{bmatrix}, \tag{24}$$

with $k_{xz} = k_{zx}$ and $\mathscr{K}(\phi)$ being a given function.

According to [27], the porosity of the rock can be expressed as

$$\phi = (\phi_0 + (1-\phi_0)(C_0 - C))\ e^{-\beta\,\sigma}, \tag{25}$$

which is a generalization of Athy's law [1]. Here, $\sigma = \sigma(x,z,t)$ is the vertical effective stress

$$\sigma = s - \alpha p_f. \tag{26}$$

The standard Athy's law may be derived from a simple poro-elastic mechanical law [30] and the modification proposed in [27] basically changes the reference porosity (i.e., the porosity at $\sigma = 0$) to account for the solid-fluid conversion due to chemical reactions. Several alternative constitutive relations for porosity are present in the literature, see for instance [10, 20], which may be modified to account for degradation/deposition processes. However, we have preferred to consider in this work a relation of Athy's type because, despite its shortcomings, it is still the most widely used in engineering practice, particularly in industrial environments. By using Eq. 25, we are also neglecting viscoplastic effects; their inclusion may be the subject of a further work. Another important simplification we have made is to consider the vertical stress as the dominant stress component, and a quasi-static situation. This is true for buried almost horizontal layers and relatively low sedimentation processes. In this situation, Eq. 26 may be considered a valid approximation.

The overburden at depth z is computed as

$$s(x,z,t) = \int_z^{z_{top}(x,t)} [(1-\phi)\rho_s + \phi\rho_f]\ g\ \mathrm{d}z' + s_{top}(x,t), \tag{27}$$

where s_{top} is the weight of overlying layers and may be variable in time, while ρ_f is the density of the fluids in the pores. It is convenient to write the equivalent differential formulation:

$$\frac{\partial s}{\partial z} = -[(1-\phi)\rho_s + \phi\rho_f]\ g \quad \text{with} \quad s(x,z_{top},t) = s_{top}(t).$$

To sum up, the equations that we are dealing with are

$$\begin{aligned} \tfrac{\partial}{\partial t}(\phi\rho_w S_w) + \nabla\cdot(\phi\rho_w S_w \mathbf{u}_w) &= 0, \\ \phi S_w(\mathbf{u}_w - \mathbf{u}_s) &= -\tfrac{k_{r,w}\mathsf{K}}{\mu_w}\left(\nabla p_w - \rho_w \mathbf{g}\right), \\ \phi &= (\phi_0 + (1-\phi_0)(C_0 - C))\ e^{-\beta\,\sigma}, \\ \tfrac{\partial s}{\partial z} &= -[(1-\phi)\rho_s + \phi\rho_f]\ g, \end{aligned} \tag{28}$$

in $\Omega(t) \times (0,T)$, to be completed with a proper set of boundary and initial conditions and with an advection diffusion reaction equation for the solute concentration, or the oil saturation, using a suitable reaction rate for C.

As we have anticipated, it is convenient to solve the problem numerically in the fixed domain $\hat{\Omega}$ introduced in Section (2.1). In this reference system, since

$$\mathbf{u}_w - \mathbf{u}_s = \hat{J}^{-1}\hat{\mathsf{F}}(\hat{\mathbf{u}}_w - \hat{\mathbf{u}}_s),$$

$$\nabla p_w = \hat{\mathsf{F}}^{-T}\hat{\nabla}\hat{p}_w,$$

the Darcy Eq. 23 becomes

$$\hat{\phi}\hat{S}_w(\hat{\mathbf{u}}_w - \hat{\mathbf{u}}_s) = -\hat{J}\frac{\hat{k}_{r,w}\hat{\mathsf{F}}^{-1}\mathsf{K}(\hat{\phi})}{\mu_w}\left(\hat{\mathsf{F}}^{-T}\hat{\nabla}\hat{p}_w - \hat{\rho}_w\hat{\mathbf{g}}\right). \tag{29}$$

where $\hat{\mathbf{g}} = -g\mathbf{e}_\xi$.

Let $\hat{\mathbf{U}}_w = \hat{\phi}\hat{S}_w(\hat{\mathbf{u}}_w - \hat{\mathbf{u}}_s)$. We can write

$$\hat{\mathbf{U}}_w = -\hat{J}\frac{\hat{k}_{r,w}\widetilde{\mathsf{K}}}{\mu_w}\left(\hat{\nabla}\hat{p}_w - \hat{\rho}_w\hat{\mathsf{F}}^T\hat{\mathbf{g}}\right), \tag{30}$$

where we have set $\widetilde{\mathsf{K}} := \hat{\mathsf{F}}^{-1}\mathsf{K}(\hat{\phi})\hat{\mathsf{F}}^{-T}$, which is symmetric and positive definite because K is symmetric and positive definite.

Finally, from Eq. 12, it is straightforward to derive

$$\frac{\partial(\hat{\phi}\hat{\rho}_w\hat{S}_w\hat{J})}{\partial t} + \hat{\nabla}\cdot(\hat{\rho}_w\hat{\mathbf{U}}_w) = 0 \quad \text{in } \hat{\Omega}\times(0,T), \tag{31}$$

$$\frac{\partial\hat{s}}{\partial\xi} = -[(1-\hat{\phi})\hat{\rho}_s + \hat{\phi}\hat{\rho}_f]\,\hat{g}\hat{J} \quad \text{in } \hat{\Omega}\times(0,T). \tag{32}$$

Therefore, system (28) in $\hat{\Omega}\times(0,T)$ reads

$$\begin{array}{l} \frac{\partial(\hat{\phi}\hat{\rho}_w\hat{S}_w\hat{J})}{\partial t} + \hat{\nabla}\cdot(\hat{\rho}_w\hat{\mathbf{U}}_w) = 0 \\ \hat{\mathbf{U}}_w = -\hat{J}\frac{\hat{k}_{r,w}\widetilde{\mathsf{K}}}{\mu_w}\left(\hat{\nabla}\hat{p}_w - \hat{\rho}_w\hat{\mathsf{F}}^T\hat{\mathbf{g}}\right) \\ \hat{\phi} = (\phi_0 + (1-\phi_0)(\hat{C}_0 - \hat{C}))\,e^{-\beta\,\hat{\sigma}} \\ \frac{\partial\hat{s}}{\partial\xi} = -[(1-\hat{\phi})\hat{\rho}_s + \hat{\phi}\hat{\rho}_f]\,\hat{g}\hat{J} \end{array}, \tag{33}$$

where in the last equation ρ_s is given by Eq. 15, while ρ_f and p_f are specified depending on the application.

Once these equations are solved, one can recover $\Omega(t)$, by solving for u_{sz}

$$\begin{cases} \frac{\partial}{\partial t}((1-\phi)\rho_s) + \frac{\partial}{\partial z}((1-\phi)\rho_s u_{sz}) = Q_s & \text{in } \Omega(t)\times(0,T) \\ u_{sz} = 0 & \text{on } \partial\Omega_b \end{cases}, \tag{34}$$

where we recall that Q_s is given by Eq. 21, and integrating to obtain z,

$$\begin{cases} \frac{\partial z}{\partial t} = u_{sz} & \text{in } \Omega(t)\times(0,T) \\ z = z_0 & \text{on } \Omega(0)\times\{0\} \end{cases}. \tag{35}$$

We have assumed, for the sake of simplicity, that $\partial\Omega_b$, i.e., the bottom boundary of $\Omega(t)$, is fixed. However, we point out that the possible movement of the bottom of the domain is a datum and in the real cases it can be given by a study of the basin history.

2.3 Specialization to the case of mineral precipitation and dissolution in sandstone rocks

Here, we specialize the model to study the effect of mineral, such as quartz, cementation in sandstone rocks on the porosity and overpressure dynamics. As explained in [11], cementation can be described as the sequence of three events, i.e., the dissolution of grains into the fluid in the pores, the diffusion of the dissolved products, and the precipitation of the solute on the solid matrix of the rock.

In this case, C represents the volume fraction of precipitated mineral, and γ the dissolved mineral concentration in terms of moles per unit volume of water.

Let us derive the mass balance equation for the mineral. If $\mathscr{B}(t) \subset \Omega(t)$ is an arbitrary compact subset in the spatial configuration, $r = r(C,\gamma)$ is a source/well term which represents the dissolution/precipitation of the mineral, and $\boldsymbol{\chi}$ the mass flux through $\partial\mathscr{B}(t)$, we have that

$$\frac{\partial}{\partial t}\int_{\mathscr{B}(t)}\gamma\phi\,\mathrm{d}\Omega = \int_{\mathscr{B}(t)} r\phi\,\mathrm{d}\Omega - \int_{\partial\mathscr{B}(t)}\boldsymbol{\chi}\cdot\mathbf{n}\,\mathrm{d}A,$$

and

$$\boldsymbol{\chi} = \phi(\gamma\mathbf{u} - D\nabla\gamma),$$

where $D > 0$ is a diffusion coefficient and $\mathbf{u} = \mathbf{u}_w - \mathbf{u}_s$. Note that, given the low velocities typical of the problem of our interest, we are neglecting dispersion effects. Hence, in $\hat{\Omega}\times(0,T)$, one has

$$\frac{\partial}{\partial t}(\hat{\gamma}\hat{\phi}\hat{J}) + \hat{\nabla}\cdot\left(\hat{\phi}\hat{\gamma}\hat{\mathbf{u}} - D\hat{\phi}\hat{\mathsf{F}}^{-T}\hat{\nabla}\hat{\gamma}\right) = \hat{r}(\hat{C},\hat{\gamma})\hat{\phi}\hat{J}. \tag{36}$$

On the other hand, the dissolution/precipitation rate r causes a decrease/increase of the concentration C of the precipitated mineral, according to

$$\frac{\partial\hat{C}}{\partial t} = -V_m\hat{r}(\hat{C},\hat{\gamma})\hat{\phi}, \tag{37}$$

where V_m is the molar volume of the mineral.

Following [3], we model r as a discontinuous function of γ and C. Let us introduce the following notation:

$$x^+ := \max(0,x), \quad x^- := (-x)^+.$$

We assume that

$$r(C,\gamma) = \lambda\left(\mathrm{sign}(C)^+F(\gamma)^- - F(\gamma)^+\right), \tag{38}$$

where

$$F(\gamma) = \frac{\gamma}{\gamma_{eq}} - 1, \text{ and } \lambda = \bar{\lambda}e^{-\frac{E}{RT}} > 0, \gamma_{eq} > 0. \tag{39}$$

Here, γ_{eq} denotes an equilibrium concentration. Note that we have assumed an Arrhenius law for the reaction rate λ, which depends on a pre-exponential factor $\bar{\lambda}$, and on the absolute temperature according to an activation energy E.

Here, R is the gas constant. We observe that, if $\gamma > \gamma_{eq}$, then $F(\gamma) > 0$ and

$$r = -\lambda \left(\frac{\gamma}{\gamma_{eq}} - 1 \right) < 0.$$

In this case, precipitation occurs. On the other hand, if $\gamma < \gamma_{eq}$, then $F(\gamma) < 0$ and $r = \lambda \ \mathrm{sign}(C)^+ \left(1 - \frac{\gamma}{\gamma_{eq}}\right) \geq 0$. In this case, if $\mathrm{sign}(C) > 0$ (i.e., if some precipitated is available in the rock), dissolution occurs. Finally, in case $\gamma = \gamma_{eq}$, $F(\gamma) = 0$ and the chemical equilibrium implies $r = 0$.

Equations 36 and 37 are added to system (33) to complete the model. In this case, $\rho_f = \rho_w$ and $p_f = p_w$ are the density and pressure of water, and $\rho_d = \rho_m$ is the mineral density.

2.4 Specialization to the case of kerogen degradation in source rocks

In this section, we specialize the model to analyze how the porosity in the source rock is influenced by the thermal degradation of kerogen into oil. We deal with a simplified chemical kinetic in which a single type of kerogen generates one type of oil, yet this model can be extended to more complex kinetics. For a detailed description of the different types of kerogen and the kinetic cracking of kerogen into oil, see [26].

The breakdown of kerogen is modeled as a first-order reaction of Arrhenius-type. Let us denote with C the volumetric concentration of kerogen. Then, C evolves as

$$\frac{\partial C}{\partial t} = -k\ C \text{ in } \hat{\Omega} \times (0, T), \tag{40}$$

where the reaction rate k is given by

$$k = Ae^{-E/RT}.$$

Here, A is the Arrhenius factor, E is the activation energy, R is the gas constant, and T is the absolute temperature, which is here a given datum.

The mass conservation of the oil phase can be expressed in the fixed domain as

$$\frac{\partial(\hat{\phi}\hat{\rho}_o\hat{S}_o\hat{J})}{\partial t} + \hat{\nabla} \cdot (\hat{\rho}_o\hat{\mathbf{U}}_o) = \hat{Q}_o\hat{J} \quad \text{in } \hat{\Omega} \times (0, T), \tag{41}$$

where we have introduced the density $\hat{\rho}_o$ of the oil phase, which may depend on temperature and pressure, the oil saturation S_o

$$S_o(x, z, t) := 1 - S_w(x, z, t), \tag{42}$$

and $\hat{\mathbf{U}}_o = \hat{\phi}\hat{S}_o(\hat{\mathbf{u}}_o - \hat{\mathbf{u}}_s)$, where $\mathbf{u}_o = \mathbf{u}_o(x, z, t)$ is the oil phase velocity. Finally, Q_o is a source term that accounts for the generation of oil through the breakdown of kerogen, and corresponds to a sink term of the solid matrix mass balance equation. Hence, $Q_o = -Q_s$, where Q_s is given by Eq. 21.

To a first approximation, one can assume that the consumption of kerogen in rock only generates oil, which justifies the assumption $Q_w = 0$, stated in Section 2.2.

The relative velocity of the oil phase $\mathbf{u}_o - \mathbf{u}_s$ obeys the Darcy law, which written in the reference domain is

$$\hat{\mathbf{U}}_o = -\hat{J}\frac{\hat{k}_{r,o}\widetilde{\mathsf{K}}}{\mu_o}\left(\hat{\nabla}\hat{p}_o - \hat{\rho}_o\hat{\mathsf{F}}^T\hat{\mathbf{g}}\right) \quad \text{in } \hat{\Omega} \times (0, T). \tag{43}$$

In Eq. 43, μ_o is the viscosity of the oil phase, which may depend on temperature, and $k_{r,o}$ is its relative permeability and is a given function of S_o.

In this framework, it is necessary to add a coupling condition for the pressures of water and oil in pores, which involves the capillary pressure p_c, namely

$$p_o - p_w = p_c, \tag{44}$$

where p_c is a given function of either the oil or the water saturation.

From now on, for the sake of notation, we omit the $\hat{}$ sign on variables and differential operators. It is understood that all equations are in $\hat{\Omega} \times (0, T)$.

Under the simplifying assumption of constant densities and viscosities of water and oil, and neglecting capillary pressure, we reformulate Eqs. 33.1, 33.2, 43, 41, 44, and 42 in the so called *Global Pressure Formulation*, see [7], i.e.,

$$\begin{cases} \nabla \cdot \mathbf{U} &= \frac{Q_o J}{\rho_o} - \frac{\partial}{\partial t}(\phi J) \\ \mathbf{U} &= -J\lambda\widetilde{\mathsf{K}}(\nabla p - \mathbf{G}), \end{cases} \tag{45}$$

$$\begin{cases} \frac{\partial}{\partial t}(\rho_o\phi S_o J) & +\nabla \cdot (\rho_o\mathbf{U}_o) = Q_o J \\ \mathbf{U_o} = \frac{\lambda_o}{\lambda}\mathbf{U} & -J\frac{\lambda_w\lambda_o}{\lambda}\widetilde{\mathsf{K}}\left((\rho_w - \rho_o)\mathsf{F}^T\mathbf{g}\right), \end{cases} \tag{46}$$

where we have introduced the total velocity $\mathbf{U}$ as $\mathbf{U} := \mathbf{U}_o + \mathbf{U}_w$, $p = p_w = p_o$, the modified vector gravity $\mathbf{G}$ as

$$\mathbf{G} := \frac{\lambda_w\rho_w + \lambda_o\rho_o}{\lambda}\mathsf{F}^T\mathbf{g}, \tag{47}$$

and the total mobility λ as

$$\lambda(S_o) := \lambda_w(1 - S_o) + \lambda_o(S_o), \tag{48}$$

with

$$\lambda_\alpha(S_\alpha) := \frac{k_{r,\alpha}(S_\alpha)}{\mu_\alpha} \quad \alpha = o, w. \tag{49}$$

The Eq. 45 can be interpreted as a volume balance for the fluids—oil and water—in the rock.

Notice that the Eq. 45 are coupled with Eq. 46 through the functions λ_w and λ_o, which depend on saturation.

This formulation is convenient in our case because the constraint that the saturations must sum to one has been integrated directly into the model, and because it suggests a straightforward splitting strategy for the numerical solution.

The Eqs. 40, 45, and 46, in which $Q_o = -Q_s$, together with Eqs. 33.3 and 33.4 form a model for the source rock.

In this case, $\rho_d = \rho_k$ is the density of kerogen, which differs from that of the rock, and the density of the fluid ρ_f is

$$\rho_f = S_w \rho_w + S_o \rho_o. \tag{50}$$

2.4.1 The constitutive equations

To close the model, we also need some constitutive relations. In particular, we have to prescribe the relative permeability functions $k_{r,w}$ and $k_{r,o}$, and the permeability function $\mathscr{K}(\phi)$ in Eq. 24. In the numerical tests, we will employ the Brooks-Corey relative permeability curves in [6], namely

$$k_{r,w}(S_w) = S_w^3, \tag{51}$$
$$k_{r,o}(S_o) = S_o^2\,(1-(1-S_o)^2), \tag{52}$$

and, see [9], the following relation between permeability and porosity

$$\mathscr{K}(\phi) = \begin{cases} k_0\phi^3 & \text{if } \phi \geq 0.1 \\ \frac{100\,k_0\phi^5}{(1-\phi)^2} & \text{if } \phi < 0.1 \end{cases}. \tag{53}$$

2.5 Some remarks on the nature of the equation for the pressure

Let us assume that the densities and the viscosities of water and oil are constant. In the case of precipitation and dissolution, the volume balance of the fluids is governed by

$$\frac{\partial}{\partial t}(\phi J) + \nabla \cdot \mathbf{U}_w = 0 \qquad \text{in } \hat{\Omega} \times (0,T), \tag{54}$$

i.e., by Eq. 33.1 with $S_w \equiv 1$.

In the case of kerogen breakdown, the volume balance of the fluids in the rock in the fixed domain is given by

$$\frac{\partial}{\partial t}(\phi J) + \nabla \cdot \mathbf{U} = \frac{Q_o J}{\rho_o} \qquad \text{in } \hat{\Omega} \times (0,T), \tag{55}$$

which is the Eq. 45.1.

Let us observe that, since ϕ depends on the overburden and on pressure, C depends on the temperature, and

$$\phi J = \frac{\phi}{1-\phi}\frac{1+C-C_0}{1-C_0},$$

one has that

$$\frac{\partial(\phi J)}{\partial t} = \frac{\partial(\phi J)}{\partial p_f}\frac{\partial p_f}{\partial t} + \frac{\partial(\phi J)}{\partial s}\frac{\partial s}{\partial t} + \frac{\partial(\phi J)}{\partial T}\frac{\partial T}{\partial t}, \tag{56}$$

where in the single phase case $p_f = p_w$, and in the two-phase model p_f is equal to the global pressure, since we are neglecting p_c .

Equations 54 and 55 can be reformulated as

$$\frac{\partial(\phi J)}{\partial p_w}\frac{\partial p_w}{\partial t} + \nabla \cdot \mathbf{U}_w = -\frac{\partial(\phi J)}{\partial s}\frac{\partial s}{\partial t} - \frac{\partial(\phi J)}{\partial T}\frac{\partial T}{\partial t}, \tag{57}$$

and

$$\frac{\partial(\phi J)}{\partial p}\frac{\partial p}{\partial t} + \nabla \cdot \mathbf{U} = \frac{Q_o J}{\rho_o} - \frac{\partial(\phi J)}{\partial s}\frac{\partial s}{\partial t} - \frac{\partial(\phi J)}{\partial T}\frac{\partial T}{\partial t}, \tag{58}$$

respectively, where

$$\frac{\partial(\phi J)}{\partial p_f} = \frac{\alpha\beta\phi J}{1-\phi}, \tag{59}$$
$$\frac{\partial(\phi J)}{\partial s} = -\frac{\beta\phi J}{1-\phi}, \tag{60}$$
$$\frac{\partial(\phi J)}{\partial T} = \left(\frac{\phi}{(1-C_0)(1-\phi)} - J\frac{1-\phi_0}{1-\phi}e^{-\beta\sigma}\right)\frac{\partial C}{\partial T}. \tag{61}$$

Equations 57 and 58 highlight the parabolic nature of the Darcy's problem whenever the porosity depends on pressure.

3 Discretization: the case of mineral precipitation and dissolution

The system of equations we have presented is rather complex and non-linear. A possible approach is to solve the problem as a single non-linear system and use a global fixed point strategy like Newton or quasi-Newton iteration. This is bound to be rather costly. Moreover, it does not give the advantage of using already available solver for some of the differential problems involved, for instance the Darcy flow and the transport/saturation equations. With the objective to have a workable method in view of some future more challenging applicative problems or the extension to 3D, we have devised a splitting strategy for its solution. However, a straightforward sequential strategy has proved to be unstable, therefore the proposed algorithm contains a combination of implicit and explicit parts. A thorough mathematical analysis is out of the scope of this work, but numerical investigations, some of which are reported in this work, have shown that the method has very good stability properties. Moreover, we have investigated some conservation properties, as we will detail in the following.

We use a constant time step $\Delta t = T/N$, T being the final instant of the simulation and N the number of time steps. Given the solution at time t^n, we compute the precipitated concentration C^{n+1} and the solute in water concentration γ^{n+1}. We then compute the solid matrix density ρ_s^{n+1}, and use some fixed point iterations, to solve the coupled problem for ϕ^{n+1} and p^{n+1}. The strategy adopted is summarized in Fig. 2.

Namely, for $n = 0, \ldots, N-1$, given C^0, $\phi^{-1} = \phi^0$, σ^0, $\mathbf{U}_w^0$, p_w^0, and γ^0, we compute:

(a) **Precipitate concentration**

$$\frac{C^{n+1}-C^n}{\Delta t} = -V_m r(C^n, \gamma^n)\phi^n;$$

(b) **Solute concentration**

$$\phi^n J^n \frac{\gamma^{n+1}-\gamma^n}{\Delta t} + \nabla \cdot \left(\gamma^{n+1}\mathbf{U}_w^n - D\phi^n \mathsf{F}^{n\,-T}\nabla\gamma^{n+1}\right) + \gamma^{n+1}\frac{\phi^* J^* - \phi^n J^n}{\Delta t} = r(C^n,\gamma^n)\phi^n J^n, \tag{62}$$

where

$$\phi^* := 2\phi^n - \phi^{n-1}, \quad J^* := J(\phi^*, C^{n+1}),$$

and

$$\mathsf{F}^n = \begin{bmatrix} 1 & 0 \\ 0 & J^n \end{bmatrix}, \quad J^n := J(\phi^n, C^n);$$

(c) **Solid matrix density**

$$\rho_s^{n+1} = \frac{(1-C_0)\rho_r + C^{n+1}\rho_k}{1 - C_0 + C^{n+1}};$$

(d) ***Fixed point iterations for porosity and pressure***

For $k = 0, \ldots, K_{max}$, given $\phi_0^{n+1} := \phi^n$ and $p_0^{n+1} := p^n$, solve:

1. **Bulk pressure (overburden)**

$$\frac{\partial s_{k+1}^{n+1}}{\partial \xi} = -[(1-\phi_k^{n+1})\rho_s^{n+1} + \phi_k^{n+1}\rho_w]\, g\, J_k^{n+1},$$

where $J_k^{n+1} := J(\phi_k^{n+1}, C^{n+1})$;

2. **Effective stress**

$$\sigma_{k+1}^{n+1} = s_{k+1}^{n+1} - p_k^{n+1};$$

3. **Porosity**

$$\phi_{k+1}^{n+1} = (\phi_0 + (1-\phi_0)(C_0 - C^{n+1}))e^{-\beta\sigma_{k+1}^{n+1}};$$

4. **Darcy's problem**

$$\begin{cases} \nabla \cdot \mathbf{U}_{w,k+1}^{n+1} &= -\left.\frac{\partial(\phi J)}{\partial t}\right|_{t^{n+1}} \\ \mathbf{U}_{w,k+1}^{n+1} &= -\frac{J_{k+1}^{n+1}}{\mu_w}\widetilde{\mathsf{K}}(\phi_{k+1}^{n+1})\left(\nabla p_{w,k+1}^{n+1} - \rho_w \mathsf{F}_{k+1}^{n+1,-T}\mathbf{g}\right), \end{cases} \tag{63}$$

where

$$\mathsf{F}_{k+1}^{n+1} = \begin{bmatrix} 1 & 0 \\ 0 & J_{k+1}^{n+1} \end{bmatrix};$$

5. **Verify stopping criteria**

(e) **Final updating**

$$\phi^{n+1} = \phi_k^{n+1}, \quad p^{n+1} = p_k^{n+1}, \quad \mathbf{U}_w^{n+1} = \mathbf{U}_{w,k+1}^{n+1};$$

We consider a conforming and regular triangulation of $\hat{\Omega}$ and proceed with the space discretization of the aforementioned equations. We have used a regular and structured triangulation because we are considering a simple configuration, focusing on one single sedimentary layer without faults, and synthetic heterogeneities. However, the methods can be implemented on arbitrary conforming triangulations.

We have chosen a mixed finite element method for both the Darcy's problem and the equation for the solute concentration. This allows us to use the same finite element approximation for the water velocity $\mathbf{U}_w$ in Eqs. 62 and 63. The finite element space chosen for the water velocity is the lowest order Raviart Thomas $\mathbb{R}\,\mathrm{T}_0(\hat{\Omega},\ \mathscr{T}_h) \subset H(\mathrm{div},\hat{\Omega})$, while the solute concentration γ and the water pressure p are in the space of the piece-wise constant functions $\mathbb{P}_0(\hat{\Omega},\ \mathscr{T}_h) \subset L^2(\hat{\Omega})$. For more details on these finite ele-ment spaces and their properties, the interested reader may consult [5, 8].

We point out that, to avoid non conservative interpolations, since the discretization of the map between the physical and the fixed domain is piecewise-linear, both deformation gradient and the jacobian are consistently discretized with piecewise-constant $\mathbb{P}_0$ elements. Moreover, the use of mixed formulation for the Darcy's and the advection-diffusion problems allows us to use a locally conservative approximation of the velocity.

In both equations, the Dirichlet boundary conditions are naturally included in the weak formulation, while the Neumann boundary conditions are imposed with a Nitsche's penalization technique (see [21]). Finally, the equation for the bulk pressure s is solved with a SUPG stabilized finite element method [16, 23], using $\mathbb{P}_1$ elements.

4 Discretization: the case of oil generation

For the case of oil generation from kerogen, we are deal-ing with a two-phase flow. Therefore, the algorithm requires some modifications. We propose a time discretization based on a splitting of the problem. Being T the final instant of the simulation, we use a constant time step $\Delta t = T/N$. For all $n = 0, \ldots, N-1$, given the solutions at the instant n, we first compute the concentration of kerogen C^{n+1}, which only depends on the concentration at the previous instant. We then compute a prediction S_o^* of the saturation, which

is obtained by solving the saturation Eq. 46 for $\phi J\, S_o$, and by dividing that solution by a prediction, via linear extrapolation of ϕ^n and ϕ^{n-1}, of the product $\phi^{n+1}J^{n+1}$, that is $\phi^* J^*$. When ϕ^{n+1} are J^{n+1} are available, a correction of the saturation is performed, exploiting the fact that

$$\phi^{n+1}J^{n+1}S_o^{n+1} = \phi^* J^* S_o^*.$$

Now, having C^{n+1} and S_o^*, we have enough information to compute the solid matrix density ρ_s^{n+1} and a prediction ρ_f^* of the fluid density. With a fixed point iteration, we then solve the strongly coupled problem for ϕ^{n+1} and p^{n+1}. At the end of these iterations, we can correct the saturation and the fluid density, as explained above. The strategy adopted is summarized in Fig. 3.

Namely, for $n = 0, \ldots, N-1$, given C^0, $\phi^{-1} = \phi^0$, σ^0, $\mathbf{U}^0$, p^0, and S_o^0, we perform the following steps.

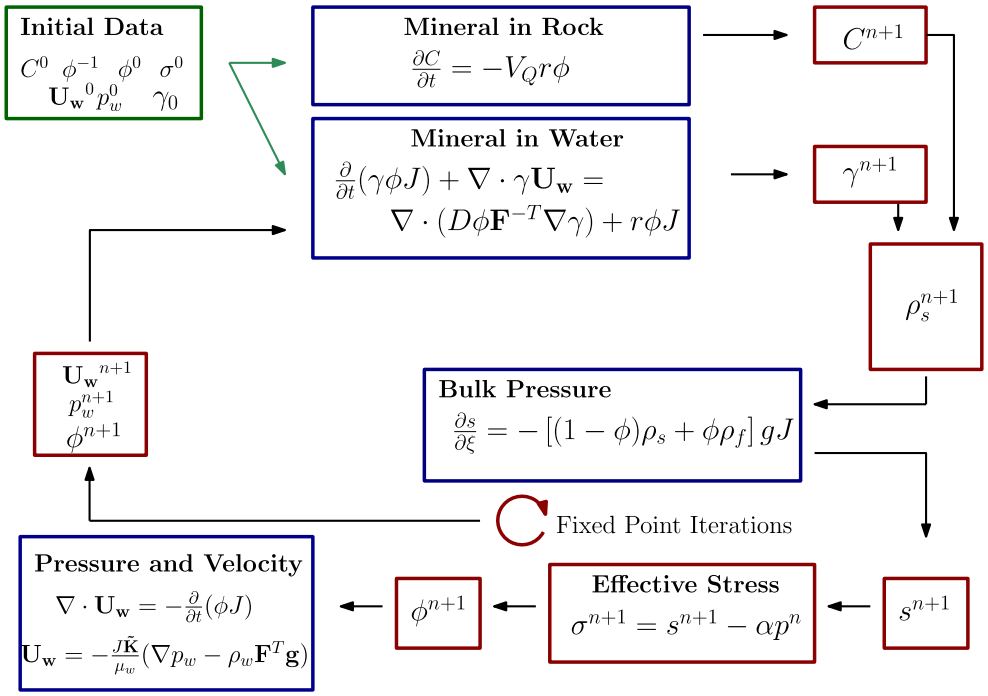

Fig. 2 Splitting strategy to solve the problem with the mineral

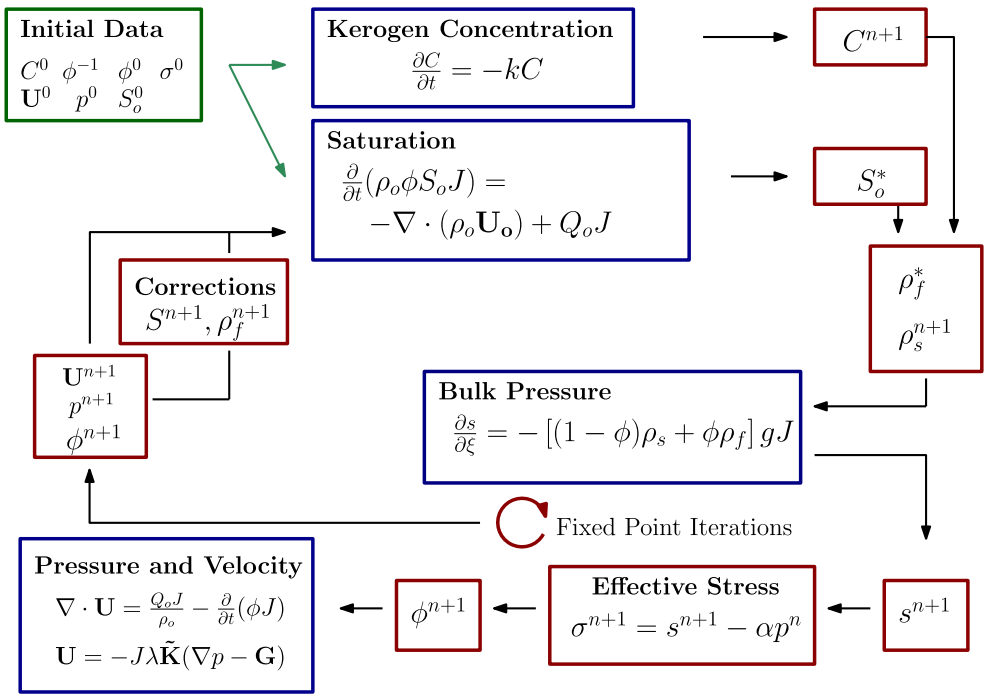

Fig. 3 Splitting strategy to solve the problem with kerogen

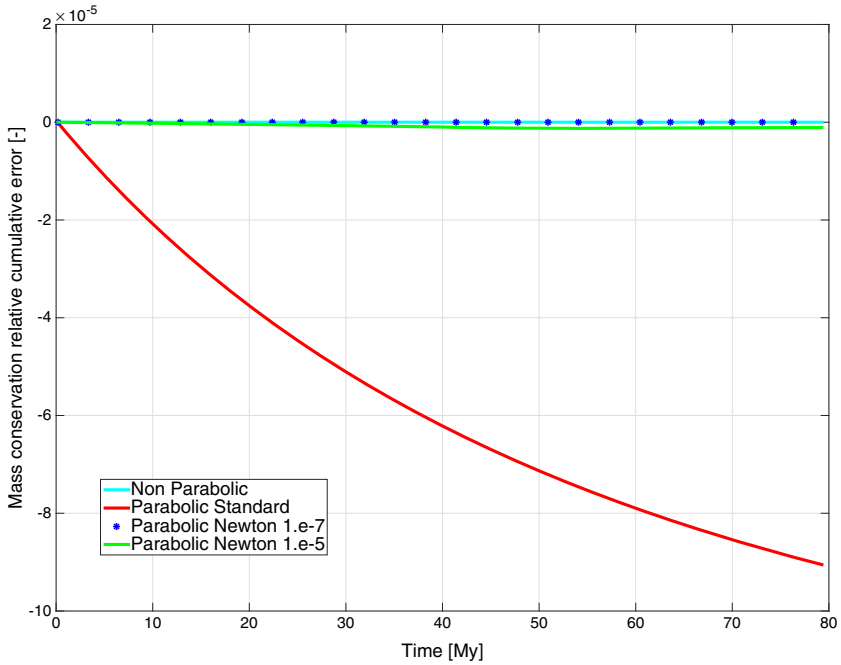

Fig. 4 Mass conservation error relative to the initial mass of water obtained with the discussed methods. The Newton parabolic method was tested with two different values of TOL_{mc}, i.e., 10^{-7} and 10^{-5}

(a) **Kerogen concentration**

$$\frac{C^{n+1} - C^n}{\Delta t} = -k\, C^{n+1};$$

(b) **Prediction of saturation**

$$\frac{\phi^* J^* S_o^* - \phi^n J^n S_o^n}{\Delta t} \rho_o = -\nabla \cdot (\rho_o \mathbf{U}_o^n) + (Q_o J)^{n+1},$$

where

$$\phi^* := 2\phi^n - \phi^{n-1}, \quad J^* := J(\phi^*, C^{n+1}), \quad J^n := J(\phi^n, C^n);$$

(c) **Prediction of the fluid density**

$$\rho_f^* = S_o^* \rho_o + (1 - S_o^*)\rho_w;$$

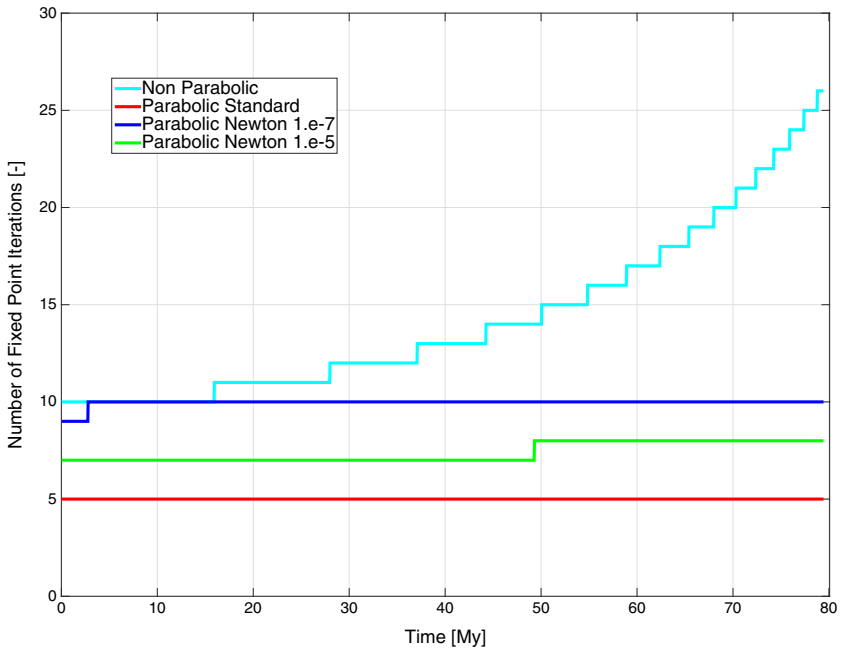

Fig. 5 Number of fixed point iterations obtained with the discussed methods. The Newton parabolic method was tested with two different values of TOL_{mc}, i.e., 10^{-5} and 10^{-7}

Table 1 Relative mass conservation errors at the end of the simulation. TOL_{mc} is the required tolerance on the relative mass conservation error at the end of the simulation

Non parabolic	3.3e-13
Parabolic standard	−9.0e-5
Parabolic Newton with TOL_{mc} = 1.e-5	1.1e-6
Parabolic Newton with TOL_{mc} = 1.e-7	−1.0e-8

(d) **Solid matrix density**

$$\rho_s^{n+1} = \frac{(1-C_0)\rho_r + C^{n+1}\rho_k}{1-C_0+C^{n+1}};$$

(e) ***Fixed point iterations***

For $k = 0, \dots, K_{max}$, given $\phi_0^{n+1} := \phi^n$ and $p_0^{n+1} := p^n$, compute:

1. **Bulk pressure**

$$\frac{\partial s_{k+1}^{n+1}}{\partial \xi} = -[(1-\phi_k^{n+1})\rho_s^{n+1} + \phi_k^{n+1}\rho_f^*]\, g\, J_k^{n+1},$$

where $J_k^{n+1} := J(\phi_k^{n+1}, C^{n+1})$;

2. **Effective stress**

$\sigma_{k+1}^{n+1} = s_{k+1}^{n+1} - p_k^{n+1}$;

3. **Porosity**

$\phi_{k+1}^{n+1} = (\phi_0 + (1-\phi_0)(C_0 - C^{n+1}))e^{-\beta\sigma_{k+1}^{n+1}}$;

4. **Darcy's problem**

$$\begin{cases} \nabla\cdot\mathbf{U}_{k+1}^{n+1} = \frac{(Q_o J)^{n+1}}{\rho_o} - \left.\frac{\partial(\phi J)}{\partial t}\right|_{t^{n+1}} \\ \mathbf{U}_{k+1}^{n+1} \quad = -J_{k+1}^{n+1}\lambda(S_o^*)\widetilde{\mathbb{K}}(\phi_{k+1}^{n+1})\left(\nabla p_{k+1}^{n+1} - \mathbf{G}\right); \end{cases} \tag{64}$$

5. **Test stopping criteria**

Table 2 Physical parameters for the simulation

	Value	Unit		Value	Unit
β	10^{-8}	Pa^{-1}	ϕ_0	0.5	–
d_0	2000	m	$\frac{\partial d}{\partial t}$	100	m/My
T_0	20	°C	$\frac{\partial T}{\partial z}$	0.035	°C/m
k_0	10^{-6}	Darcy	g	9.81	m/s^2
μ_w	0.001	Pa s	D	1.58 10^{-8}	m^2/s
ρ_w	1000	kg/m^3	V_m	0.0226	m^3/mol
ρ_m	2660	kg/m^3	ρ_r	2500	kg/m^3
$\bar{\rho}$	2500	kg/m^3	γ_{eq}	0.167	mol/m^3
E	60.1	kJ/mol	$\bar{\lambda}$	8.37 10^{-6}	mol/(m^3 s)

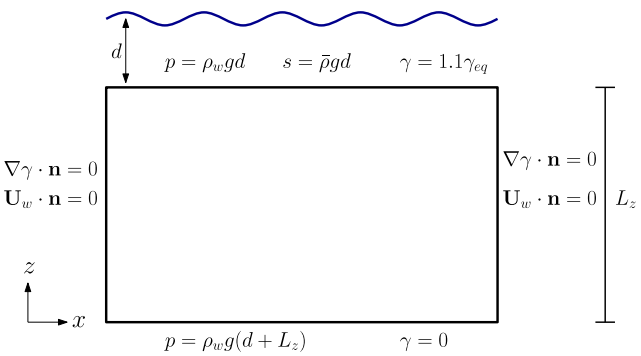

Fig. 6 A sketch of the boundary conditions for the problem of mineral precipitation and dissolution. Notice that the domain represented in the sketch is the initial domain $\Omega(0)$, while the problem is solved in $\hat{\Omega}$. The density $\hat{\rho}$ represents an average of the overlying material densities

(f) **Fixed point updating**

$$\phi^{n+1} = \phi_{k+1}^{n+1}, \quad p^{n+1} = p_{k+1}^{n+1}, \quad \mathbf{U}^{n+1} = \mathbf{U}_{k+1}^{n+1}$$

(g) **Correction of the saturation**

$$S_o^{n+1} = \frac{\phi^* J^*}{\phi^{n+1} J^{n+1}} S_o^*$$

(h) **Correction of the fluid density**

$$\rho_f^{n+1} = S_o^{n+1}\rho_o + (1 - S_o^{n+1})\rho_w;$$

As in the previous case, we adopt a mixed finite element method $\mathbb{RT}_0 - \mathbb{P}_0$ for the space discretization of the global pressure-velocity system, and a SUPG stabilized finite element method for the equation for the bulk pressure. The saturation equation is solved with the Godunov method, which guarantees by construction the oil phase mass conservation, and the time step is chosen such that the CFL condition holds.

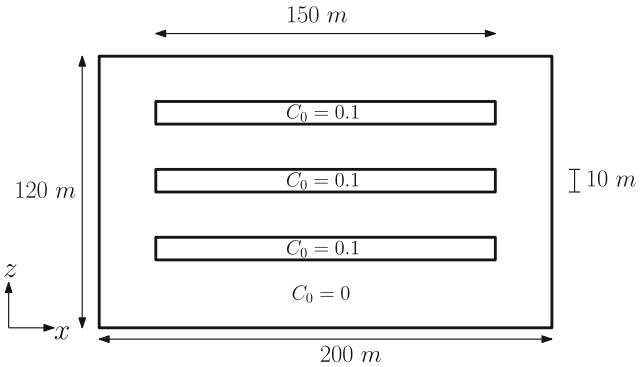

Fig. 7 A sketch of the initial domain $\Omega(0)$, and the initial precipitated mineral concentration

Fig. 8 The mineral concentration in rock at $t = 0$ My, $t = 15$ My, $t = 30$ My, $t = 45$ My, and $t = 60$ My

5 Approximation of the fluid mass balance equation

A relevant issue is the approximation of the term $\frac{\partial(\phi J)}{\partial t}\Big|_{t^{n+1}}$ in Eqs. 63 and 64. In fact, the different discretizations of this term have an impact on the approximation of the mass conservation for the fluids and on stability.

Indeed, we have verified that an explicit discretization of $\frac{\partial \phi J}{\partial t}$ using quantities available at the previous steps leads to stability problems in the fixed point iterations in both the case of mineral precipitation/dissolution and that of kerogen breakdown. One possibility is then to solve (63) and (64) in their parabolic forms (57) and (58), respectively. This choice has proven to be very good for stability, but it does not assure mass conservation at the numerical level, unless Eq. 56 holds also at the discrete level. A technique that assures good stability and numerical mass conservation, consists of linearizing the equation with respect to pressure. More

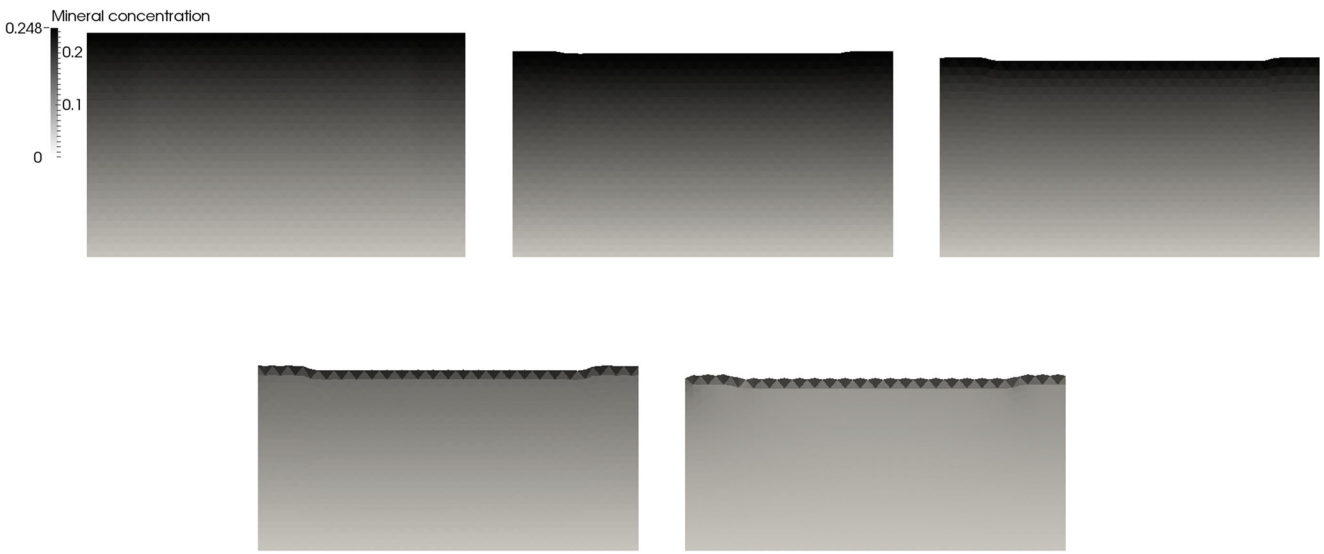

Fig. 9 The mineral concentration in solution at $t = 0$ My, $t = 15$ My, $t = 30$ My, $t = 45$ My, and $t = 60$ My

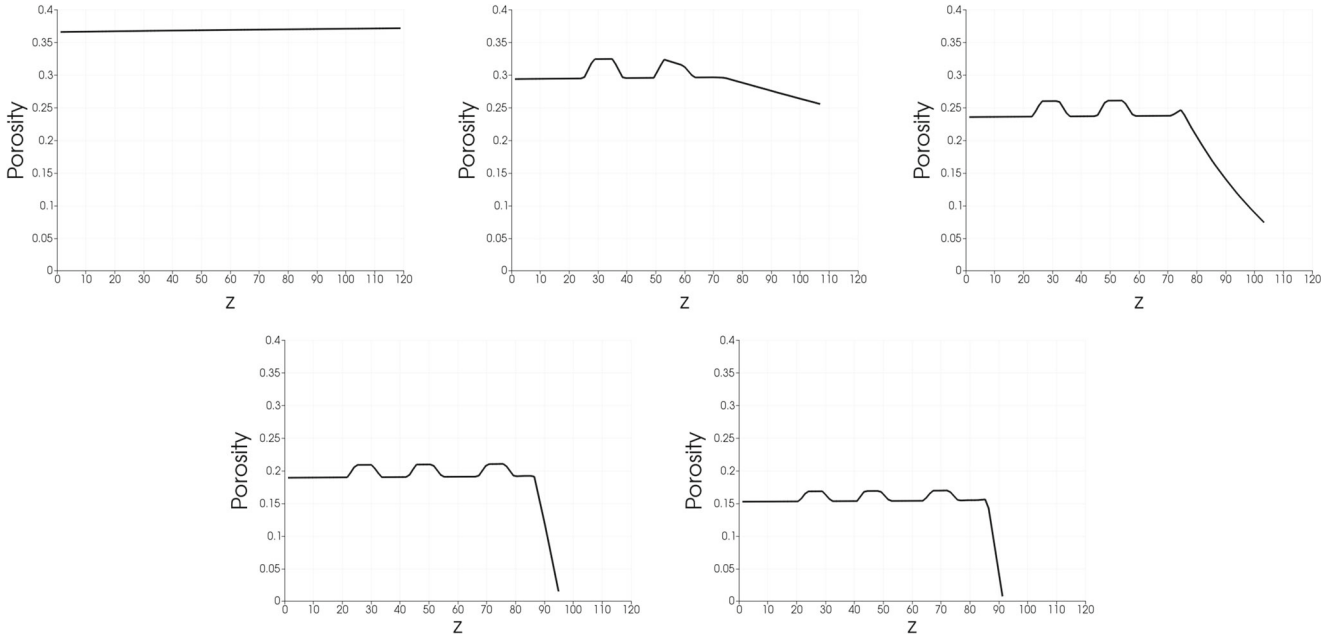

Fig. 10 Plot of porosity versus z at $t = 0$ My, $t = 15$ My, $t = 30$ My, $t = 45$ My, and $t = 60$ My, taken on the vertical line that halves the domain

precisely, in the case of mineral precipitation and dissolution at each time step t^{n+1}, we solve the following nonlinear equation for p_w^{n+1}

$$\nabla \cdot \mathbf{U}_w^{n+1} + \frac{(\phi J)^{n+1}(p_w^{n+1}) - (\phi J)^n}{\Delta t} = 0.$$

By applying Newton linearization, recalling Eq. 59, we obtain

$$\alpha\beta \frac{\phi_{k+1}^{n+1} J_{k+1}^{n+1}}{1 - \phi_{k+1}^{n+1}} \frac{p_{w,k+1}^{n+1} - p_{w,k}^{n+1}}{\Delta t} = -\nabla \cdot \mathbf{U}_{w,k+1}^{n+1} - \frac{\phi_{k+1}^{n+1} J_{k+1}^{n+1} - (\phi J)^n}{\Delta t}.$$

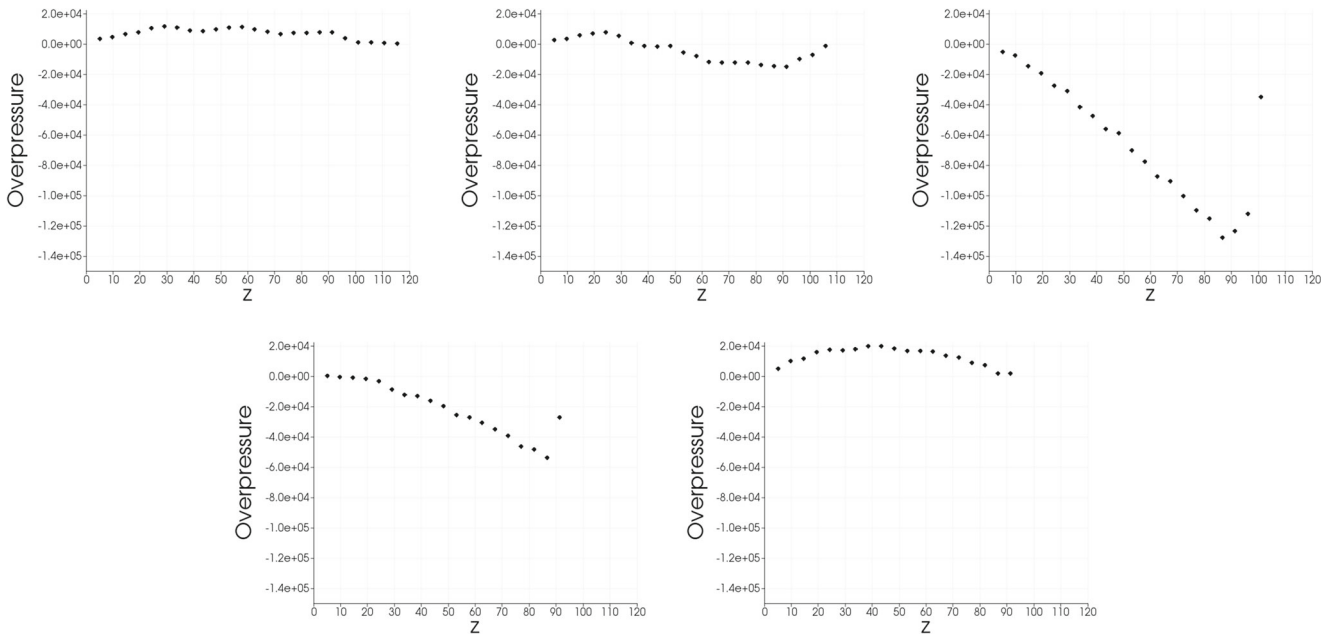

Fig. 11 Plot of the overpressure versus z at $t = 0$ My, $t = 15$ My, $t = 30$ My, $t = 45$ My, and $t = 60$ My, taken on the vertical line that halves the domain

Table 3 Physical parameters for the simulation

	Value	Unit		Value	Unit
β	10^{-8}	Pa^{-1}	ϕ_0	0.5	-
d_0	2000	m	$\frac{\partial d}{\partial t}$	50	m/My
T_0	20	°C	$\frac{\partial T}{\partial z}$	0.035	°C/m
k_0	10^{-6}	Darcy	g	9.81	m/s^2
μ_w	0.001	Pa s	μ_o	0.001	Pa s
ρ_w	1000	kg/m^3	ρ_o	750	kg/m^3
ρ_k	1150	kg/m^3	ρ_r	2500	kg/m^3
$\bar{\rho}$	2500	kg/m^3	A	10^{12}	1/s
E	200	kJ/mol	R	8.31	J/(K mol)

With this approach, we can obtain discrete mass conservation at the same time, up to a fixed tolerance depending on Δt. In fact, the absolute conservation error per time step is

$$\left| \int_{\hat{\Omega}} \left(p_{w,k+1}^{n+1} - p_{w,k}^{n+1} \right) \frac{\alpha\beta\phi_{k+1}^{n+1} J_{k+1}^{n+1}}{1-\phi_{k+1}^{n+1}} \, \mathrm{d}\hat{\Omega} \right| =$$

$$\left| \int_{\Omega(t^{n+1})} \left(p_{w,k+1}^{n+1} - p_{w,k}^{n+1} \right) \frac{\alpha\beta\phi_{k+1}^{n+1}}{1-\phi_{k+1}^{n+1}} \, \mathrm{d}\Omega \right| \leq$$

$$|\Omega(0)||p_{w,k+1}^{n+1} - p_{w,k}^{n+1}|\alpha\beta \frac{\phi_0}{1-\phi_0}.$$

Hence, using the tolerance tol on the pressure increment between consecutive fixed point iterations as stopping criterion induces a tolerance TOL_{mc} on the conservation error at the end of the simulation, i.e., when $t = T$, relative to the initial volume V_0, such that

$$tol = TOL_{mc} \, \frac{V_0}{\alpha\beta L_x L_z} \, \frac{1-\phi_0}{\phi_0} \, \frac{\Delta t}{T}.$$

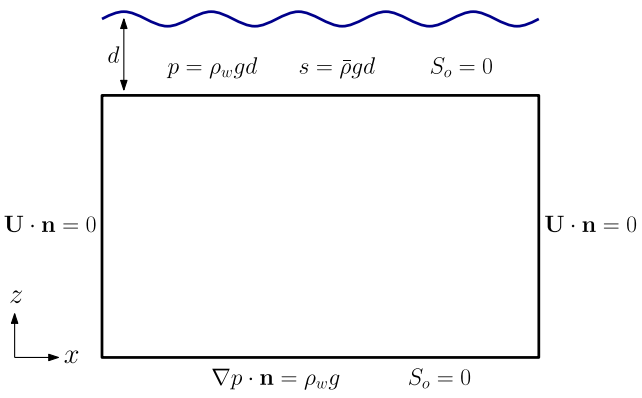

Fig. 12 A sketch of the boundary conditions for the problem of kerogen. Notice that the domain represented in the sketch is the initial domain $\Omega(0)$, while the problem is solved in $\hat{\Omega}$. The density $\hat{\rho}$ represents an average of the overlying material densities

Having set TOL_{mc}, we can compute the tol that we should use to stop the fixed point iterations, which, fixed the final time of the simulation, depends linearly on Δt. Notice that we have considered a volume balance, under the assumption of constant densities.

The same argument, with the proper modifications due to the presence of the oil source term, holds in the case of kerogen breakdown.

An example is given in Figs. 4 and 5, where we show the mass conservation error relative to the initial mass of water, and the number of fixed point iterations performed as a function of time, for a simplified problem of pure mechanical compaction. Hence, the three methods discussed can be summarized as follows:

– **Non parabolic**

$$\nabla \cdot \mathbf{U}_{w,k+1}^{n+1} = -\frac{\phi_{k+1}^{n+1} J_{k+1}^{n+1} - \phi^n J^n}{\Delta t}, \tag{65}$$

– **Standard parabolic**

$$\frac{\alpha\beta\phi_{k+1}^{n+1}}{\left(1-\phi_{k+1}^{n+1}\right)^2} \frac{p_{k+1}^{n+1} - p^n}{\Delta t} + \nabla \cdot \mathbf{U}_{w,k+1}^{n+1} = \frac{\beta\phi_{k+1}^{n+1}}{\left(1-\phi_{k+1}^{n+1}\right)^2} \frac{s_{k+1}^{n+1} - s^n}{\Delta t}, \tag{66}$$

– **Newton parabolic**

$$\begin{aligned} &\frac{\alpha\beta\phi_{k+1}^{n+1}}{\left(1-\phi_{k+1}^{n+1}\right)^2} \frac{p_{k+1}^{n+1}-p^n}{\Delta t} + \nabla \cdot \mathbf{U}_{w,k+1}^{n+1} = \\ &-\frac{\phi_{k+1}^{n+1} J_{k+1}^{n+1} - \phi^n J^n}{\Delta t} + \frac{\beta\phi_{k+1}^{n+1}}{\left(1-\phi_{k+1}^{n+1}\right)^2} \frac{p_k^{n+1}-p^n}{\Delta t}. \end{aligned} \tag{67}$$

Note that the right hand side of Eq. 67 is an approximation of $-\frac{\beta\phi J}{1-\phi} \frac{\partial s}{\partial t}$, according to Eq. 56. Also, Eq. 67 reduces to Eq. 65 at convergence of the fixed point iteration.

The figures show the results for the non parabolic and standard parabolic methods and for the Newton-linearized parabolic method, for two different values of TOL_{mc}. We observe that the non parabolic method is the one that best conserves mass, but it is not stable, in the sense that a large, growing number of iterations is required. On the other hand, the standard parabolic method is the

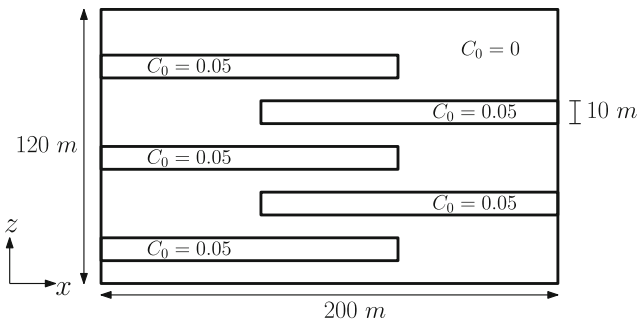

Fig. 13 A sketch of the initial domain $\Omega(0)$, and the initial kerogen concentration

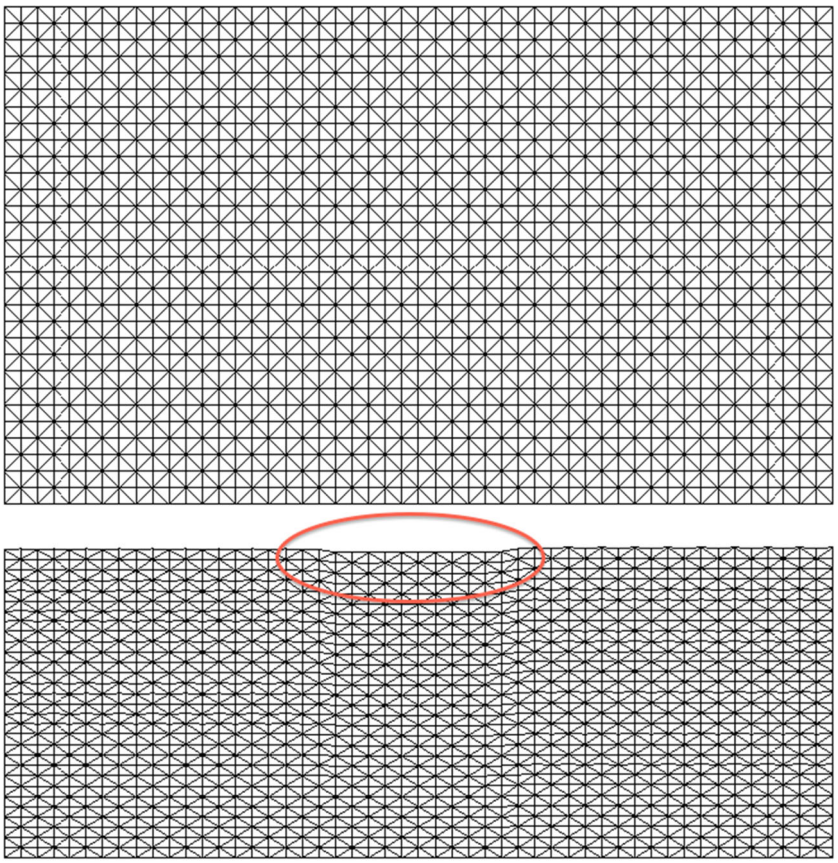

Fig. 14 The initial domain $\Omega(0)$ (at the *top*) and the fixed domain $\hat{\Omega}$ (at the *bottom*). Notice the extra compaction of $\hat{\Omega}$ in the center, due to the greater amount of kerogen in that region than in the neighborhood (see Fig. 13 for the initial kerogen concentration field)

less expensive method in terms of computational effort, but the mass conservation error diverges during the simulation. The Newton-linearized parabolic method proves to be a very good compromise, with the advantage that the desired tolerance of mass conservation error can be arbitrarily set. In Table 1, we report the relative mass conservation errors at the end of the simulation, for each method.

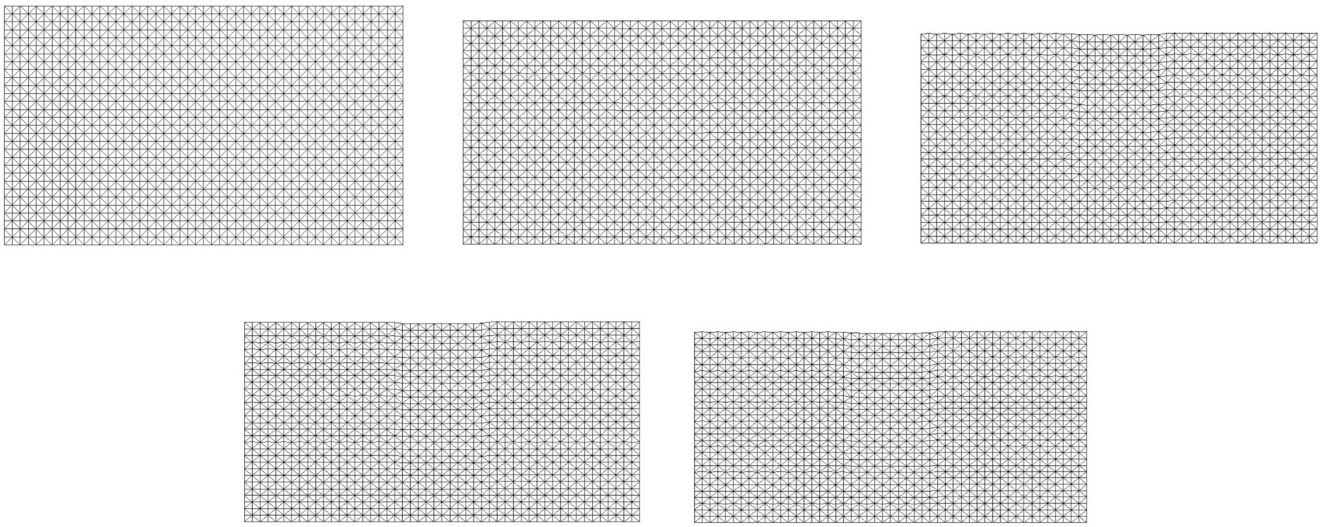

Fig. 15 The physical domain $\Omega(t)$ at $t = 0\ My$, $t = 20\ My$, $t = 40\ My$, $t = 60\ My$, and $t = 80\ My$. Notice that most of the kerogen breaks down approximately between $t = 20\ My$ and $t = 30\ My$. This is why in the second figure, in which little kerogen breakdown has happened, one can only observe mechanical compaction and the domain is still rectangular

Fig. 16 Kerogen concentration at $t = 0\ My$, $t = 20\ My$, $t = 40\ My$, $t = 60\ My$, and $t = 80\ My$. Kerogen vanishes before half simulation

6 Numerical results: the case of mineral precipitation and dissolution

In this section, we simulate the dynamics of dissolution and precipitation of a mineral species in a sedimentary layer. At the beginning of the simulation the domain is a 200 m $\times$ 120 m rectangle, at the depth d_0 = 2000 m. We have used a triangular mesh 50 $\times$ 30 and a time step $\Delta t = 10^{12}\ s \approx 30\ ky$ to simulate a time span of $T = 60$ My.

A constant sedimentation velocity $\frac{\partial d}{\partial t}$ = 100 m/My is imposed. The temperature is a given field that corresponds to a surface temperature of 20 °C and a geothermal gradient $\frac{\partial T}{\partial z}$ equal to 3.5 °C per hundred meters. The main physical parameters are reported in Table 2.

In Fig. 6, the boundary conditions are summarized. Concerning pressure, we have set an hydrostatic Dirichlet condition at the top of the domain and at the bottom. No-flux conditions are imposed on the lateral edges, since the domain is considered as a part of a longer thin layer of

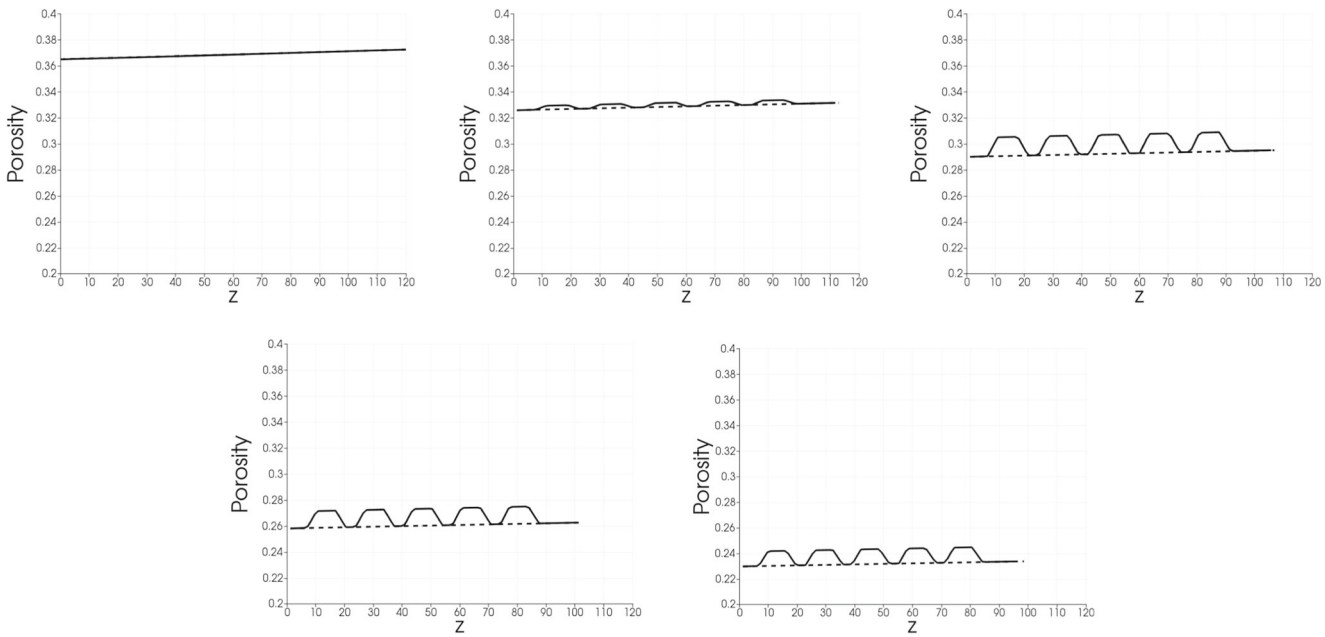

Fig. 17 Plot of porosity versus z at t = 0 My, t = 20 My, t = 40 My, t = 60 My, and t = 80 My, taken on the vertical line that halves the domain. The *dashed line* shows porosity when we have no kerogen, while the *solid line* shows porosity when the initial concentration of kerogen is that of Fig. 13

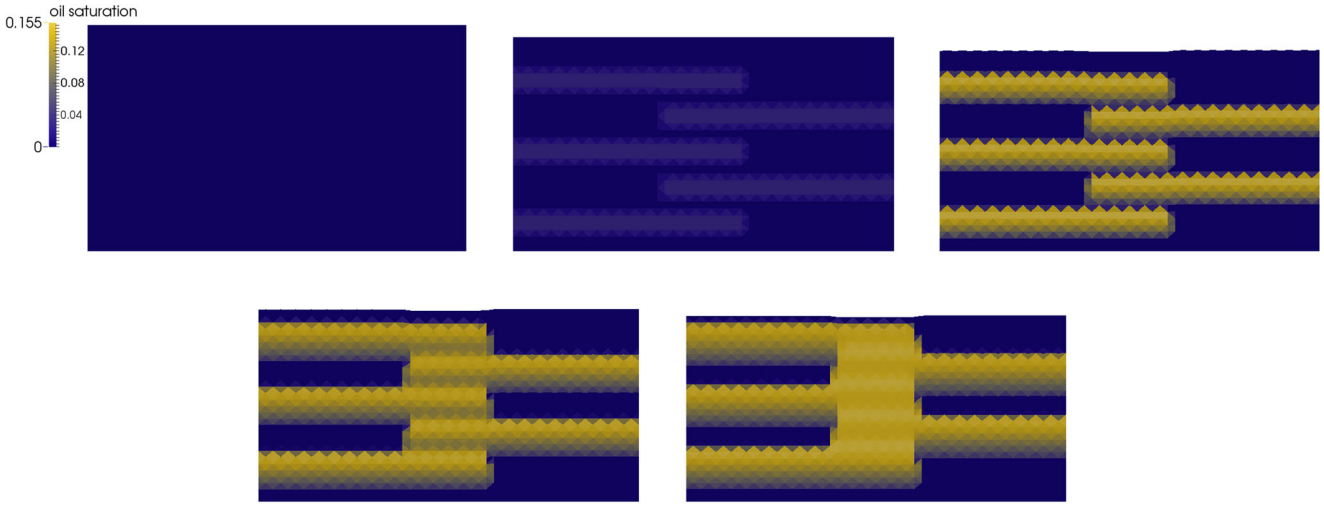

Fig. 18 The oil saturation at $t = 0$ My, $t = 20$ My, $t = 40$ My, $t = 60$ My, and $t = 80$ My

rock, lying along the x-direction. Finally, we set a Dirichlet condition for the bulk pressure at the top, due to the overburden, and we assume that the bottom of the domain moves downwards with a given, and in our case uniform, velocity.

The boundary conditions for both overload and pressure are time-dependent due to the progressive burial of the domain, during the 60 My of simulation.

The rock is initially filled with water with no mineral dissolved ($\gamma = 0$). The initial condition for pressure is the hydrostatic pressure and the initial conditions for stress and porosity are computed with some fixed point iterations of the stationary problem. The initial distribution of the precipitated mineral in the rock is sketched in Fig. 7. Finally, $\mathbf{U}_w^0 = \mathbf{0}$ and $\phi^{-1} = \phi^0$. Notice that, as pointed out in Section 3, we need two initial conditions for porosity.

Since the initial concentration of mineral in water is zero, the precipitated mineral in rock starts to dis-solve, as shown in Fig. 8. The water flow transports the dissolved mineral upwards, where, since we have set $\gamma \geq \gamma_{eq}$ as a boundary condition, it precipitates again in the rock and reducing considerably the porosity, as shown in Figs. 9 and 10. Notice, also, that porosity is higher where the precipitate concentration was non-zero at the initial time,

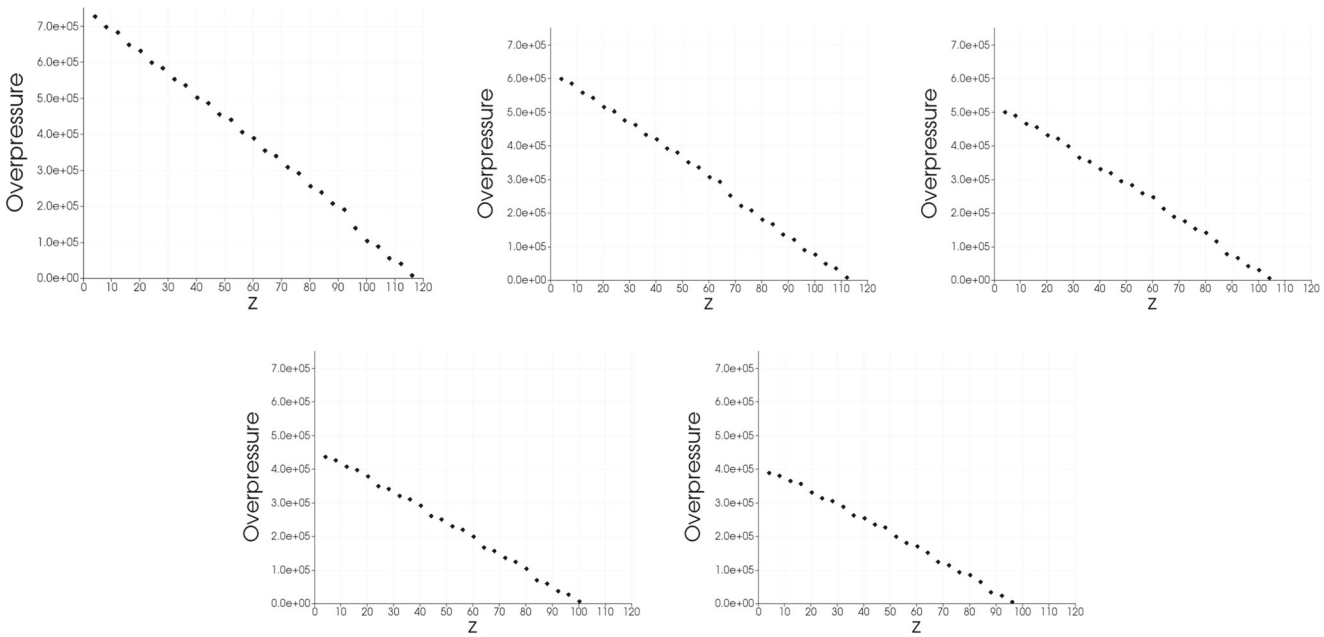

Fig. 19 Plot of the overpressure versus z at $t = 0$ My, $t = 20$ My, $t = 40$ My, $t = 60$ My, and $t = 80$ My, taken on the vertical line that halves the domain

since the dissolving mineral leaves some void spaces. In Fig. 9, we can observe that the dissolved mineral flows out of the domain transported by water. In Fig. 11, the overpressure is shown, which, after a transitory, gets back in the end of the simulation close to the initial, almost negligible, value.

7 Numerical results: the case of kerogen

In this section, we simulate the dynamics of oil generation and expulsion in a portion of source rock. At the beginning of the simulation the domain is a 200 m $\times$ 120 m rectangle, at the depth d_0 = 2000 m. We have used a triangular mesh 50×30 and a time step $\Delta t = 10^{12}\ s \approx 0.03$ My to simulate a time span of T = 80 My.

A sedimentation velocity $\frac{\partial d}{\partial t}$ = 50 m/My is imposed. The temperature, necessary to trigger the chemical reaction of kerogen degradation, is, as in the previous section, a given field that corresponds to a surface temperature of 20 °C and a geothermal gradient $\frac{\partial T}{\partial z}$ equal to 3.5 °C per hundred meters. The main physical parameters of the simulation are reported in Table 3.

In Fig. 12, the boundary conditions are summarized. Concerning pressure, we have set the same conditions as in Section 6, except for the bottom of the domain, where an hydrostatic gradient Neumann condition was set. Moreover, if we assume that the velocity of the oil phase outside the source rock is much higher than that inside the domain, coherently with the higher permeabilities expected there, we can assume that only water is present at the top and bottom boundaries. Notice that the boundary conditions for saturation on the side boundary are redundant, since $\mathbf{U} \cdot \mathbf{n} = 0$ there and $\mathbf{g} \cdot \mathbf{n} = 0$ in our case. Finally, the boundary condition for the bulk pressure at the top and that on the bottom of the domain are the same discussed in Section 6.

The sedimentation of the layers above the domain during the 80 My of simulation leads to a progressive burial of the domain, which causes the boundary conditions for both overload and pressure to change.

We point out that having at disposal a full scale study of the basin would allow us to choose more realistic pressure boundary conditions at the bottom.

The rock is initially filled with water and the oil saturation is $S_o^0 = 0$. The initial condition for pressure is the hydrostatic pressure and the initial conditions for stress and porosity are computed with some fixed point iterations of the stationary problem. The distribution of the kerogen in the source rock is sketched in Fig. 13. Finally, $\mathbf{U}^0 = \mathbf{0}$. Notice that, as pointed out in Section 4, we need two initial conditions for porosity, thus we take $\phi^{-1} = \phi^0$.

In Fig. 15, we can clearly observe the progressive compaction of the physical domain, which is greater in the regions where the initial kerogen concentration was on average higher. In Fig. 14, we represent the fixed domain $\hat{\Omega}$, which is computed at the beginning of the simulation. The occurrence of compaction can also be observed in Fig. 17, as ϕ decreases significantly from the beginning to the end of the simulation in the whole domain.

During the simulation, the burial of the domain caused by sedimentation makes the temperature increase until—after about 20 My—kerogen breakdown occurs. In Fig. 16, we can observe the consumption of kerogen, which totally vanishes before 40 My.

In Fig. 17, we compare the porosity obtained considering hydrocarbons generation (shown in the solid line) with the porosity obtained with the same data but neglecting kerogen consumption (shown in the dashed line). We can observe that in the region where kerogen was initially located, the porosity is higher than in the surroundings. Also, in the regions where no kerogen was initially present, the porosities in the two cases coincide. We can clearly see how the breakdown of kerogen causes an extra porosity, which will then be subject to compaction until, in the end, the differences due to the different kerogen concentrations are less noticeable. However, it can be observed in Fig. 14 that the thickness of the layer in the fixed configuration is slightly smaller in the center of the domain, where C_0 was larger.

At the same time, as kerogen is consumed, oil saturation increases, as shown in Fig. 18, until enough oil is present to be able to move in the source rock. In Fig. 19, the overpressure is shown which is small and decreases with time.

8 Conclusions

We have developed a mathematical model, as well as a numerical discretization strategy, that aims at providing a general framework for the study of geochemical compaction. Indeed, it is formulated to take into account chemical reactions that can reduce the porosity, as in the case of the deposition of minerals, or increase the porosity, for instance because of the dissolution of solid grains. These effects are always coupled with the mechanical compaction resulting from the balance between overload and pore pressure. Since the model is formulated for the two-phase flow case, and the single phase flow can be obtained as a particular case, it is also suitable for the simulation of the particular diagenetic processes of oil generation due to the conversion of solid organic matter. From the numerical point of view, we propose an iterative splitting strategy for the solution of the coupled problem of fluid flow, mechanical compaction, and chemical reactions. Although fully coupled approaches are more robust, they result in very large and ill conditioned

schemes. Moreover, in the view of realistic simulations, one could easily use pre-existing tools for each of the sub-problems in an iteratively coupled framework. We assessed the performances of this strategy in terms of convergence (number of fixed point iterations) and mass conservation. The results show that the discretization of the mass balance equation plays a critical role: indeed, a naive discretization where the time derivative of the porosity acts as a source terms leads to stability problems, while a discretization that highlights the parabolic nature of the Darcy problem in a compressible medium is stable but not mass conservative. We propose a discretization strategy based on the linearization of the parabolic problem where mass conservation can be fulfilled up to a desired tolerance defined by the user, in a compromise between accuracy and computing time. Despite the simplifying assumptions, the proposed test cases give qualitatively correct results. Future developments of this work may include more realistic reaction schemes as well as more realistic geometries with strong heterogeneities, such as fractures, in the domain.

Acknowledgments We gratefully acknowledge E&P division of Eni S.p.A. for partially supporting this research.

References

1. Athy, L.F.: Density, porosity, and compaction of sedimentary rocks. AAPG Bull. **14**(1), 1–24 (1930)
2. Biot, M., Willis, D.: The elastic coefficients of the theory of consolidation. ASME Journal of Applied Mechanics pp. 594–601 (1957)
3. Bouillard, N., Eymard, R., Herbin, R., Montarnal, P.: Diffusion with dissolution and precipitation in a porous medium: mathematical analysis and numerical approximation of a simplified model. ESAIM: Math. Model Numer. Anal. **41**, 975–1000 (2007)
4. Brezis, H.: Functional analysis, Sobolev spaces and partial differential equations. Springer, New York (2011)
5. Brezzi, F., Fortin, M.: Mixed and hybrid finite element methods. Springer, New York (2012)
6. Brooks, R.H., Corey, A.T.: Hydraulic properties of porous media. Civil Engineering Dept., Colorado State Univ., Fort Collins, CO (1964)
7. Chavent, G., Jaffré, G.: Mathematical models and finite elements for reservoir simulation. Elsevier Science Publishers B.V (1986)
8. Chen, Z.: Finite element methods and their applications. Springer, New York (2005)
9. Chen, Z., Ewing, R.E., Lu, H., Lyons, S.L., Maliassov, S., Ray, M.B., Sun, T.: Integrated two-dimensional modeling of fluid flow and compaction in a sedimentary basin. Comput. Geosci. **6**, 545–564 (2002)
10. Coussy, O.: Poromechanics. John Wiley & Sons (2004)
11. Formaggia, L., Guadagnini, A., Imperiali, I., Lever, V., Porta, G., Riva, M., Scotti, A., Tamellini, L.: Global sensitivity analysis through polynomial chaos expansion of a basin-scale geochemical compaction model. Comput. Geosci. **17**, 25–42 (2013)
12. Formaggia, L., Nobile, F.: A stability analysis for the arbitrary Lagrangian Eulerian formulation with finite elements. East-West J. Numer. Math. **7**, 105–131 (1999)
13. Fowler, A., Yang, X.s.: Fast and slow compaction in sedimentary basins. SIAM J. Appl. Math. **59**(1), 365–385 (1998)
14. Fowler, A., Yang, X.s.: Pressure solution and viscous compaction in sedimentary basins. J. Geophys. Res. **104**(B6), 12,989–12,997 (1999)
15. Fowler, A., Yang, X.S.: Dissolution/precipitation mechanisms for diagenesis in sedimentary basins. J. Geophys. Res. Solid Earth (1978–2012) **108**(B10) (2003)
16. Franca, L., Frey, S.L., Hughes, T.J.: Stabilized finite element methods: I. application to the advective-diffusive model. Comput. Methods Appl. Mech. Eng. **95**(2), 253–276 (1992)
17. Ismail-Zadeh, A., Krupskii, D.P.: Extrusion and gravity current of a fluid: Implications for salt tectonics. Physics of the Solid Earth **42**, 999–1006 (2006)
18. Lander, R.H., Walderhaug, O.: Predicting porosity through simulating sandstone compaction and quartz cementation. AAPG bull. **83**(3), 433–449 (1999)
19. Longoni, M., Malossi, A.C.I., Quarteroni, A., Villa, A., Ruffo, P.: An ALE-based numerical technique for modeling sedimentary basin evolution featuring layer deformations and faults. J. Comput. Phys. **230**, 3230–3248 (2011)
20. Nedjar, B.: Formulation of a nonlinear porosity law for fully saturated porous media at finite strains. Journal of the Mechanics and Physics of Solids **61**(2), 537–556 (2013)
21. Nitsche, J.: Über ein Variationsprinzip zur Lösung von Dirichlet-Problemen bei Verwendung von Teilräumen, die keinen Randbedingungen unterworfen sind. Abhandlungen aus dem Mathematischen Seminar der Universität Hamburg **36**, 9–15 (1971)
22. Pang, X., Jiang, Z., Zuo, S., Lerche, I.: Dynamics of hydrocarbon expulsion from shale source rocks. Energy, Exploration & Exploitation **23**(5), 333–355 (2005)
23. Quarteroni, A., Valli, A.: Numerical approximation of partial differential equations. Springer, Berlin (2008)
24. Scotti, A.: A numerical model for generation, retention and expulsion of hydrocarbons from source rock. Ph.D. thesis, Politecnico di Milano (2010)
25. Suetnova, E.: Vasseur, G.: 1-D modelling rock compaction in sedimentary basins using a visco-elastic rheology. Earth Planet. Sci. Lett. **178**, 373–383 (2000)
26. Vandenbroucke, M.: Kerogen: from types to models of chemical structure. Oil & Gas Sci. Technol. **58**(2), 243–269 (2003)
27. Wangen, M.: Vertical migration of hydrocarbons modelled with fractional flow theory. Geophys. J. Int. **115**, 109–131 (1993)
28. Wangen, M.: Two-phase oil migration in compacting sedimentary basins modelled by the finite element method. Int. J. Numer. Anal. Methods Geomech. **21**, 91–120 (1997)
29. Yang, X.S.: Nonlinear viscoelastic compaction in sedimentary basins. Nonlinear Process. Geophys. **7**, 1–7 (2000)
30. Yang, X.S.: A unified approach to mechanical compaction, pressure solution, mineral reactions and the temperature distribution in hydrocarbon basins. Elsevier Tectonophysics **330**, 141–151 (2001)